Labeling of white matter of MRI brain images using skeleton

by

Mohsen Taghaddosi

A thesis submitted in partial fulfillment of the requirements for the degree of

Master of Science

Department of Computing Science

University of Alberta

Abstract

Image segmentation is the problem of assigning 2D pixels or 3D voxels to a set of finite labels. In particular, in medical imaging, the goal of segmentation is to partition an MRI or CT image into regions that are relevant to the biology of a particular disease, for example the motor cortex in Amyotrophic Laterals Sclerosis (ALS).

This thesis studies the problem of segmenting T1 MR images of a human brain into a set of predefined regions. Heretofore, many methods have been proposed for brain segmentation into anatomical structures, some of which use a set of manually labeled brain images to guide the segmentation. These methods use the intensity of each voxel to calculate the best transformation which registers images into a single common space and then they apply the same transformation to the labeled images to get the final results.

Our work is based on extracting the skeleton (medial axis) of white matter and use it to choose an image from a set of images in a training data set that are manually labeled by experts. Then we use that information to register the input image and then apply the same transformation to the labeled image to achieve an estimation of the final result. Finally, a refining optimization step is done by applying an optimization to improve the results.

Our experiments on a data set shows that our proposed method outperforms current methods in terms of accuracy and also its time complexity is very efficient.

Acknowledgements

I would like to thank my supervisors, Professor Herbert Yang and Sanjay Kalra for their invaluable guidance, encouragement and patience throughout this thesis. I cannot imagine this project done without their incredible support.

I would also like to thank all my friends at University of Alberta for being supportive and making my life easy in graduate school. Lastly, I thank my family whom I can always count on.

Table of Contents

List of Tables

List of Figures

Chapter 1

Introduction

There are many applications in medical imaging and neuroscience that need anatomical information of different parts of a human brain. After the invention of high quality cross-sectional imaging techniques such as Magnetic Resonance Imaging (MRI) and Computed Tomography (CT), a significant improvement in medical diagnosis and disease prevention has been made [38].

Cerebral tumor detection is an example of medical imaging applications which has the ability to distinguish between soft tissues of a human brain [68]. The amount of data generated in an imaging method is more than what can be analyzed visually, so there is a need for automatic methods of image analysis. Segmentation is the first step in data extraction of an MRI image [40]. By image segmentation, an image is divided into different tissues or segments based on some given criteria [17]. Medical applications such as surgical planning, post-surgical assessment, abnormality detection, etc. depend on medical image segmentations [17]. Automated image registration methods are widely used in medical imaging. Image registration is the process of aligning two or more images, in order to find the best labeling of interested structures of the input image. Fusion of anatomical images with functional images is one of the applications of image registration, which demonstrates the importance of image registration [60].

Although scientists discovered different functional regions of a human brain, no two brains are identical and each brain has different shapes which require a lot of training and knowledge for experts to locate a specific region in a brain. Segmentation is an important stage in the detection of brain morphology variability

and in 3D visualization for surgical planning [45]. The complexity of the brain structure affects the effectiveness of segmentation, which makes it very difficult, if not impossible. Because of the complexity of segmenting the brain, there is no defined method to choose a good segmentation algorithm. To compensate for the lack of robustness caused by the variability of the brain, approaches like region-based segmentation, registration with a deformable atlas and deformable models have been proposed [5].

A diseases that corresponds to degeneration of neurons is Amyotrophic Lateral Sclerosis (ALS). In this disease, the upper and lower motor neurons (UMN and LMN) are damaged progressively. Patients who are suffering from ALS disorder have a median life span of three years [98]. The upper motor neurons are located in the precentral gyrus which includes functionality of the primary motor cortex in Broadmann's area number 4 [13]. Therefore, a key point in diagnosing this disease is to locate the gyri accurately. The challenge of making a diagnoses of ALS is the lack of a reliable biomarker. Recently, texture analysis methods on brain images have been proposed to detect ALS in the brain MRI [57], [84].

As stated earlier, the problem of segmenting brain images into anatomical structures is still a difficult task in the medical imaging field. In this thesis we aim to focus on four regions in the upper part of the brain which are the superior frontal gyrus, the superior parietal lobule, the precentral gyrus and postcentral gyrus. These four regions are shown in Figure 1.2.

In neuroanatomy, a gyrus is a ridge and a sulcus is a depression or groove in the cerebral cortex. Sucli and Gyri are surrounding each other and they form the folded appearance of the brain in human and mammals. The sulci and gyri are depicted in Figure 1.1 [26].

The definitions of these four regions adapted from [25] are as follows:

1. "Superior Frontal Gyrus: The rostral boundary of the superior frontal gyrus is the rostral extent of the superior frontal sulcus, and the caudal boundary is the paracentral sulcus on the inflated surface. The medial and lateral boundaries are designated as the medial aspect of the frontal lobe and the superior frontal sulcus, respectively."

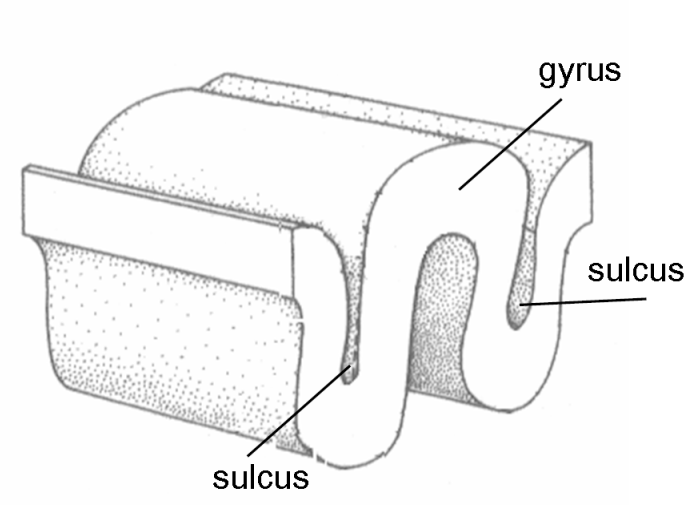

Figure 1.1: Sulco-gyral structures of the human cerebral cortex

2. Superior Parietal Lobule: ”The rostral and caudal boundaries of the superior parietal cortex were the precentral gyrus and lateral occipital cortex, respectively. The medial and lateral boundaries were the precuneus and/or cuneus cortex and the inferior parietal cortex, respectively.”

3. Precentral Gyrus: The gyrus immediately rostral to the central sulcus.

4. Postcentral Gyrus: The gyrus immediately caudal to the central sulcus.

Currently there are several registration and segmentation methods which use machine learning algorithms by providing manually labeled MRI images done by experts as a training data set for image registration. As well, some methods use one atlas while others several atlases have been proposed to segment the brain MRI into anatomical regions [93]. Some of the applied methods for image segmentation include simple thresholding, region growing, fuzzy C-means, Markov random field models and FFT based segmentation [7]. The registration is done by finding the best transformation between the input image and every single subject in the training data set, or a weighted average of training subjects. The transformation is usually calculated by optimizing a cost function defined based on the differences between the source and target image intensities.

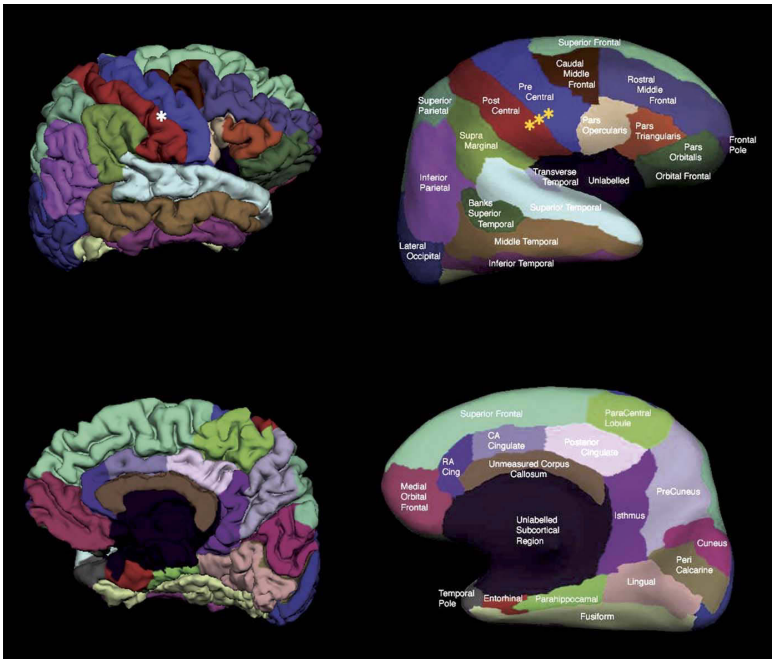

Figure 1.2: Anatomical regions in human brains [25]

Image registration in medical imaging can be performed by applying the publicly available software packages and source codes such as FAIR [58], AIR [90], ITK [96], etc. There are several comparative studies which compare several image registration methodologies [88]-[95].

Classification of image registration methodologies can be performed based on different criteria such as the dimensionality of the data, nature of the registration basis, domain of transformation, etc. Image registration methods are also categorized based on features such as intensity gradient, statistical information of voxel intensity, etc. [60]. The disadvantages of existing methods for registration are that they are not very robust against noise and usually, they require several sequential steps such as skull removal, denoising, intensity normalization, etc. to obtain acceptable results. By increasing the number of steps the chance of error propagation increases. Furthermore, manual intervention is required at some point to correct the error.

The main contribution of this thesis is to simplify the structure of a human brain by calculating the skeleton of white matter in 2D slices and then use it to register and segment different regions of the brain. The main advantage of the proposed

method is the efficient running time and robustness against noise.

The rest of the thesis is organized as follows. In chapter 2 we review the concepts of medical imaging and discuss different methods of current registration and segmentation methods. In chapter 3, we present the proposed method to calculate the skeleton of white matter and discuss how to utilize that information to find the transformation between the input image and training samples. Then we evaluate our method and compare it to one of the state of the art registration methods in chapter 4. Finally, in chapter 5 we conclude this thesis.

Chapter 2

Background

In this chapter, a review of the methods proposed to segment the brain images into anatomical regions is summarized. There are two parts in the review: 1) an overview of CT and MRI techniques and 2) a review of related works of our research area which includes segmentation and registration. MRI and CT are cross-sectional imaging techniques which have the ability to create high-quality three-dimensional images of the brain or other internal organs of the human body [12]. Imaging methods play a significant role in medical diagnosis and disease prevention [38].

2.1 CT Scanning

X-ray computed tomography (X-ray CT) is a medical imaging method using X-ray radiation. In this method X-ray is emitted to a target organ from different angles. A cross-sectional image is produced by applying the computer processing methods to rays from specific area of the organ. This process provides visibility of the internal organs. Since the introduction of CT, it has become an indispensable tool in medical imaging. CT scanning of the lungs and the head are some examples of applications of this imaging method in diagnoses [12].

2.2 MRI Technique

In MRI, the imaging procedure is done using strong magnetic fields and radio waves. For this reason MRI is preferred to CT as the latter which uses harmful ionizing radiation [38]. However, CT also has advantages against MRI, such as

lower cost and shorter time for imaging. MRI has contraindications like for those who with a cardiac pacemaker and it is a time consuming method [12]. MRI is a popular imaging method with many applications in medical diagnosis, especially in brain imaging. Analysis of MRI images of brain tissues can be used to detect tumors because of its ability to differentiate soft tissues [68]. The distinction between tissues arises from the difference in relaxation times of different tissues. Also recording of lung motion with high temporal resolution can be performed using dynamic two-dimensional magnetic resonance imaging (2D-MRI) [79]. MRI has made impressive development in recent years, specially with improvements in image quality and speed of acquisition strategies [49], [76].

The performance of MRI performance depends on excitation and relaxation of protons. In this process the radio waves are directed at protons. Under the influence of the magnetic field, the protons are excited and then relaxed. As a result of proton relaxation, radio signals that are emitted from protons are used to create an image. Proton relaxation occurs with a specific constant time which depends on the tissue, so we can distinguish between different types of tissue such as white and gray matter of the brain [68].

2.2.1 MRI Sequences

An MRI sequence consists of a number of radiofrequency pulses and gradients that form the image. Different types of sequences can be used in MRI and the obtained contrast between tissues relies on the applied pulse sequences [51]. The density of protons in an area determines the darkness or brightness of the resulting image. T1 and T2 are times which are related to the relaxation time of protons and the obtained images from these two times are different, e.g. in T1-weighted images grey matter is darker than white matter, while it is brighter than white matter in T2-weighted images.

The contrast between the white and gray matter of brain T1-weighted images is better than that of T2-weighted images. Both types of sequences can reveal tumors. Tumors are shown as dark areas in T1-weighted images and as bright areas in T2-weighted images. Because of the fundamental differences between T1 and

T2 scans, understanding the basics of these scans is essential to achieve the desired results. Decision about the type of scan is related to what is required in the final image [68].

2.2.2 MRI Usages

An MRI scan reveals details of the structure of the human brain. Detection of cortical changes associated with some illnesses or normal aging process is possible using MRI. Furthermore, MRI is a useful tool for identifying the responses of patients with a brain disease to treatments. Alzheimer's disease (AD) and multiple sclerosis (MS) are two examples of diseases in which MR images are used to help for diagnosis. MRI measurements are used in clinical research on patients suffering from AD. There are several methods for automated quantification of regions of interest (ROI), but these methods do not have clinical application [25].

Desikan et al. proposed an automatic labeling system for classifying the human cerebral cortex into regions of interest. The MRI scans of subjects suffering from brain abnormalities such as tumors and infarcts were utilized in the automatic labeling procedure. T1-weighted gradient echo sequence was used in this approach. Identification of cortical ROIs was performed by both manually and automatic methods in each of the individual hemispheres. Manual identification was used for assessing the validity of the automated labeling system. Intraclass correlation coefficient (ICC) was considered as a parameter for validity evaluation. The results of this research show high accuracy of automated ROIs, with an average ICC of 0.835 which confirmed the validity of the proposed automated method for subdividing the human cerebral cortex to 34 cortical ROIs [25].

2.3 Registration

Automated image registration (AIR) methods are widely used in medical applications. Image registration is to align two or more images, in order to find the optimal transformation that best matches the structures of interest of the input image. Most of the research in the field of medical image analysis was dedicated to image reg-

istration and this fact demonstrates the importance of image registration. Fusion of anatomical images obtained from CT or MRI images with functional images from PET and fMRI is one of the applications of image registration. Medical image registration has been frequently used for the brain as well as for other anatomical parts of the human body [60].

Image registration methodologies can be classified based on different criteria; the following are some of these criteria:

1. Dimensionality of the data (1D, 2D, 3D)
2. The features used in the registration process (intrinsic or extrinsic properties of the patients)
3. Transformation domain (local or global)
4. Transformation elasticity (rigid, projective or curved)
5. Interaction (automatic, semi-automatic or interactive)

In addition to these criteria, image registration methods are also categorized based on the feature space information. This information may be the intensity gradient, statistical information of the voxel intensity and derived information from structures extracted from the input image. Broadly speaking, image registration methods can be classified into intensity based and feature based methods [60].

The diagram shown in Figure 2.1 demonstrates an overview of intensity based registration methodologies. The process of searching for geometric transformation continues until the optimized transformation is found. The similarity measure (relevant to voxel density) is calculated in the overlapped regions of the image to be registered. Interpolation is used to resample the voxel intensity using the geometric transformation between the transformed image and the reference image. If possible, a pre-registration transformation is used as the first step in order to make the moving image close to the fixed image. This action can speed up the process of finding the optimizer [60].

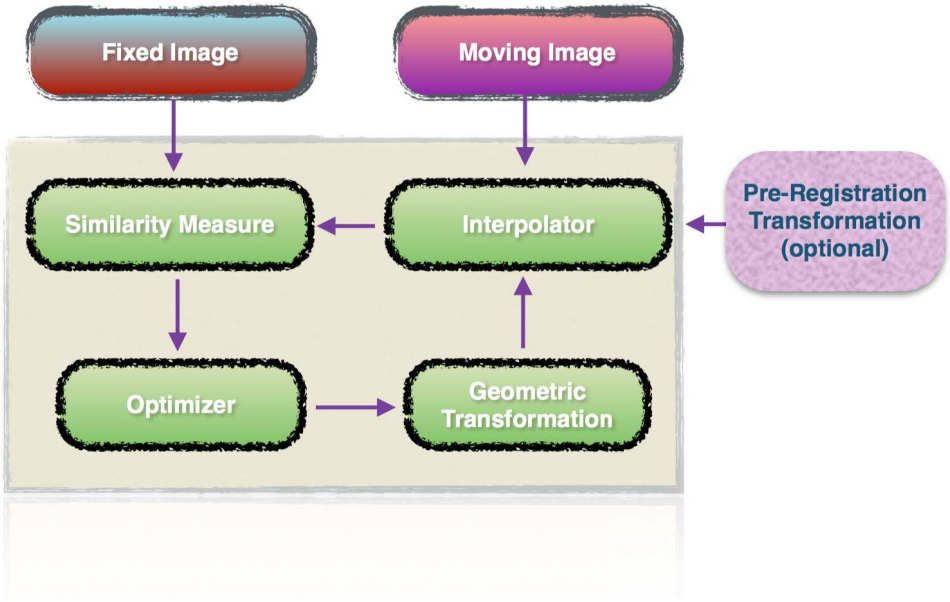

Figure 2.1: An overview of intensity based registration methodologies [4]

2.3.1 Geometric Transformation

The geometric transformations can be divided into two categories of "rigid" and "non-rigid". A rigid transformation can be described by 6 degrees of freedom (DOF) in a 3D space: 3 translational and 3 rotational DOFs. The non-rigid transformation class includes the similarity transformation (translation, rotation and uniform scaling), affine (translation, rotation, scaling, and shear), projective, and curved. The curved transformation is also commonly referred to as a deformable, elastic or fluid transformation. The rigid and similarity geometric transformations are subsets of the affine transformation [60]. According to the literature, a rigid geometric transformation is mainly applied to two situations. One is in the registration of rigid structures, such as bones and the other is in pre-registration before a more complex geometric transformation.

Since most organs and anatomical parts of a human body are deformable, medical image registration is performed using curved deformation. Free-form transformations and guided deformations are two types of curve deformation which have

been applied to medical images. In most of the free-form deformation models, a set of control points is determined and these points are moved in order to optimize a similarity measure. Cubic B-spline is the most widely used curve to specify the transformation between control points [60].

Kelin et al. compared the surface-base a brain image registration and the volume-based one for the first time. In their study, they selected FreeSurfer and Spherical Demons for surface registration and SyN[4] and ART[1] for volume based registration. They performed more than 16000 registrations between 40 brain images, either directly to each other or through templates, with the brains represented as either volumes or as surfaces [47].

To evaluate accuracy of registration, the authors employed manually labeled images. To evaluate registration performance, they used a permutation test of top-ranked volume and surface registration methods and compared the selections with one another. After registration they confirmed that removing non-brain matter would help brain volume registration. They found out that custom-made optimal average templates improve registration over direct pairwise registration, and that resampling errors introduced by converting volume labels to surfaces or surface labels to volumes can be used to make a fair comparison between volume and surface registration methods using present resampling methods [47].

Wood et al. proposed an AIR method to register MRI images [91]. The main characteristics of their method are:

1. It does not require explicit information of anatomical features and allows any selection of registration target.

2. It is robust to varying voxel intensities within the brain.

3. It does not need user interactions except for removing the scalp, skull and dura.

4. The user can choose between different sets of linear and nonlinear spatial transformation models.

5. Their transformation models are invariant to rotation, translation, and scaling.

6. The implementation of their algorithm is available.

The AIR algorithm consists of several iterations and the user can choose the number of iterations for doing the registration. At first, a global rescaling parameter is added to achieve 7 degrees of freedom for rigid body transformation. The next transformation is the 9 parameters Talairach model, a special case of the general affine model. The affine linear model is used at the third iteration which has 12 parameters and is invariant to rotation, translation and scaling [91].

At the fourth step, a second order polynomial model is used in comparison to the affine model which is the first order polynomial model (linear). The second order polynomial model has 30 parameters. The order of polynomials is increased to the fifth order to refine the registration accuracy. The total number of parameters for the last step is 168. At each step a coarse to fine estimation method is used to resample the data and the sampling step is increased by applying improvements in the cost function [91].

ANIMAL (Automated Nonlinear Image Matching and Anatomical Labelling) is a 3D method proposed by Collins et al. for registering and labeling MRI images using a manually labelled atlas [21]. Their proposed method uses blurred image intensity and image gradient magnitude as input features to be invariant in terms of translation, rotation and scaling. They compute these features by convolving the input image with zeroth and first order 3D isotropic Gaussian derivatives. The whole process is done hierarchically in which spatial registration is refined from a blurry image to a more detailed version of that. For the nonlinear part of their method, they used local deformations fields to find the best transformation that maximizes the similarity based on normalized correlation between the input image and the atlas. [21].

They apply the inverse transformation on the manually labelled atlas to decide the label of each voxel of the input image. Since the calculation of registration is totally independent of the labelled atlas, the users can provide arbitrary manually segmented brain images to do the segmentation [21].

Chiang et al. proposed a registration method based on an information theoretic measure which is the Jensen-Renyi Divergence (JRD) of the input and the template

image [18]. JRD was used for image registration before them with linear rigid transformation in [65] and they extended this work to nonlinear registration. In their proposed method, the driving force is iteratively calculated at each voxel in such a way that the JRD value between the template and the input image is minimized with viscous fluid regularization constraint.

2.4 Brain Tissue Segmentation

Segmentation plays a significant role in many medical applications, for instance, abnormality detection [63], schematization of surgery [71] and surgical assessment[83]. Also, functional and structural brain imaging play a considerable role in neuroscience. The amount of data generated by an imaging method is not easy to be analyzed manually. Hence, there is a need for an automatic method of image analysis. Segmentation- which partitions an image into desired regions or segments and is the first step in information extraction from an image. So far, many methods have been developed for the segmentation of an image [40], [39].

Image processing techniques have been developed in recent years and have influenced the advancement of medical imaging. MR imaging is the most important tool to detect brain abnormalities such as tumors, which demonstrates the importance of accurate segmentation [7]. Nowadays, all medical imaging methods are done digitally [17] which will magnify the importance of image segmentation as one of the most important steps in image processing and computer vision applications. By image segmentation, the image is divided into different parts based on some given criteria [17].

Representative methods for segmentation of MRI of the brain can be divided into two categories: **basic tissue classification** and **anatomical segmentation procedures**. Since images taken by MRI preserve the required information to distinguish between different portions of the brain such as white and gray matter, tissue classification methods can be done automatically. However, automatic anatomical segmentation is difficult because anatomical differences do not necessarily lead to difference in relaxation times and hence, image contrast. In other words, similar

signals can be received from tissues in different anatomical areas. This deficiency restricts the type of images that can be analyzed with anatomical segmentation methods [40].

Pixel intensity is a popular feature used in the segmentation of MR images. For example, edges and texture are calculated using intensity values. Segmentation normally refers to the grouping of pixels based on their attributes or features, which translates to finding and grouping of similar features. Successful segmentation methods depend on selecting good features [20]. An overview of edge detection methods is summarized in section 2.4.1.

Heretofore several methods have been proposed for brain segmentation into anatomical structures [93]. Using data obtained from different subjects in segmentation is called atlas-based segmentation method. Some of which use one atlas (single-atlas approach) [2] while others use more than one atlas (multi-atlas approach) [41], [87].

In the single-atlas approach we deal with an atlas made by a collection of training atlases from different subjects with the aim of finding a representative atlas that can accommodate the variability of brain structures. In single atlas methods, the segmentation process is done quickly but the accuracy can be low, especially in subjects with remarkable differences from subjects used in the atlas preparation. Because of the problems of this approach, Shiee et al. suggest a method with an adaptive atlas [93]. In their proposed method they construct a new model to use a non-stationary relaxation factor instead of a global one which helps them to segment all of the regions at once. Then they use the outcome of weighted majority voting approach as the input of their adaptive model.

In order to overcome the above mentioned problem, multi-atlas methods use a set of atlases and segmentation is performed by a label fusion approach. One of the disadvantages of multi-atlas methods is the time complexity. If the set of training atlases does not include a subject with the brain disease, the method will not be able to handle diseased brains properly [93].

According to the above discussed difficulties, it seems essential to develop an automated method with a high accuracy which can also be used in brain diseases.

Yan et al. suggested two methods of brain segmentation for different applications. The first method called extended adaptive statistical atlas (EASA) is used for healthy brain. This method segments a healthy brain into to 34 structures with high accuracy and speed [93].

In the second method, which is developed for subjects with brain diseases, the scanned image is labeled using a label fusion multi-atlas method (weighted majority voting: WMV) and then the result is used as input to EASA. The new method is called the hybrid WMV-EASA approach [93]. The accuracy of these methods is evaluated on healthy controls and subjects with Alzheimer's disease. The results in segmentation are significantly better than similar methods in segmentation [93].

One of the main problems in segmentation is the presence of noise in images that causes the failure of many segmentation techniques and hence, will affect the outcome of clinical diagnosis, which requires accuracy and precision.

2.4.1 Edge detection

Edge detection for image segmentation is one of the most important applications of soft computing techniques and is frequently used in digital image processing. An edge is defined as a boundary between two adjacent homogeneous regions and edge detection is considered as the first step of image segmentation. Senthilkumaran et al. tried to achieve a good edge detection algorithm for application in image processing and for this purpose they studied some recent soft computing approaches such as Fuzzy logic, Genetic Algorithm (GA) and Neural Network [73].

Fuzzy logic has been applied to image processing tasks in different ways. The purpose of segmentation is to classify pixels into similar regions, while Fuzzy segmentation classifies pixels into fuzzy sets. Neural networks are a family of statistical machine learning models inspired by the way information is processed by the nervous system. During the learning process, the network learns by adjusting the weights between layers so that it can predict the correct label of an incoming input. Genetic algorithms which try to mimic the evolution theory, have been used in different image processing problems such as segmentation. The main idea of these algorithms is that the only individuals that can survive and transmit their character-

istics to their descendants are the ones well adapted to their environment.

Comparison of the three most famous methods in edge detection was performed in [73]. These methods are:

1. Prewitt method
2. Robert method
3. Sobel method
4. Fuzzy method
5. Genetic algorithm method
6. Neutral Network method

Figure 2.2 represents the results of different edge detection methods.

2.4.2 Main Problems of Segmentation

The main problems that researchers deal with in segmentation are [61]:

1. Guassian noise
2. The bias field which is the inhomogeneity of voxel intensity variations across the MR image
3. The partial volume effect which is related to the resolution of MR images and happens when a voxel contains more than one tissue type [6]

Heretofore, many methods have been proposed to address these problems. Using standard filters, nonlinear filtering, Markov Random Field (MRF) models [33] and non-local means models (NL-means) [14] are examples for de-noising methods employed in medical image filtering. The performance of these methods is similar to the general noise removal methods, which requires more improvements [7].

Some of the utilized methods for image segmentation are thresholding, region growing, fuzzy C-means [36], learning vector quantization (LVQ)[7], self-organizing maps (SOM)[80], hybrid SOM (HSOM)[7], watershed [53], the active

(a) Original Image

(b) Fuzzy method

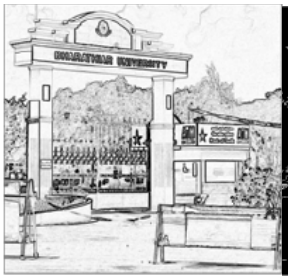

(c) Genetic algorithm method

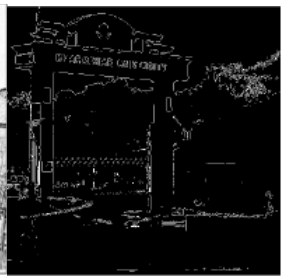

(d) Sobel method

(e) Robert method

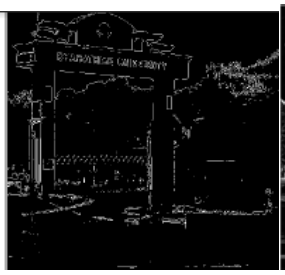

(f) Prewitt method

(g) Neutral Network method

Figure 2.2: The results of different edge detection methods [73]

control model [97], Markov random field models [54], graph cuts based methods[69], segmentation of brain with anatomical deviations [19], and FFT based segmentation [7]. A segmentation method which considers only image intensity is the fuzzy C-means (FCM), which fails when noisy image is used. However, several algorithms have been suggested to address the noise issues [7].

Atkins et al. proposed a robust automatic method for brain segmentation using magnetic resonance imaging technique [3]. Their method can be used even in an environment with radio frequency. The authors use an integrated approach which employs image processing techniques based on anisotropic filters and snakes contouring techniques developed by Snell [75]. A priori knowledge is used to remove the eyes. Their method is multistage; first of all the background noise is removed by using a head mask, next a rough outline of the brain is found, finally the final mask from rough brain outline is found [3].

Fischl et al. propose a technique for automatically assigning a neuroanatomical label to each voxel of an MR image. In contrast to existing segmentation procedures that only label a small number of tissue classes, their method assigns one of 37 labels to each voxel, including left and right caudate, putamen, pallidum, thalamus, lateral ventricles, hippocampus, and amygdala. The classification technique employs a registration procedure that is robust to anatomical variability. The proposed technique indicates that the results of neuroanatomical labeling are comparable to that manual labeling. The advantage of this technique is the detection of volume change of noncortical structures. This advantage can be used for detecting the onset of Alzheimer's disease [29].

Heckemann et al. investigated failure modes in the process of label propagation and examined the performance of label propagation with decision fusion of brain MR images. Label propagation is a procedure that prepares automated anatomical segmentation. Anatomical segmentation of an image by label propagation contains systematic and random errors. By fusing multiple labels, random error can be reduced. In other words, the accuracy of target image labeling will improve by using decision fusion which combines results from multiple segmentations [40].

The authors of [40] investigated segmentation propagation and decision fusion

methods on MR images of 30 healthy subjects. They measured the conformity between the results of automatically and manually labeling and then evaluated the accuracy of the proposed method. The labeling process is performed using a transformation derived from an atlas (a pair of an anatomical image and its relevant label) and the target image using a nonrigid registration algorithm. The transformation of the set of labels from the coordinate system of an atlas to that of the target image was performed using the acquired geometric transformation. At the end, the authors illustrated a practical procedure which increases the accuracy of the labeling process using previous methods [40].

Destrieux et al. propounded an automatic parcellation method for the localization of human cortical gyri and sulci. Parcellation strives to subdivide the cortex of the human brain into structural parts, which has a fundamental role in understanding the relationship between different brain structures and their functions [26].

Twenty-four healthy subjects were included in the study of [26]. The volunteers were scanned using MRI. Adjustable parameters for imaging were optimized so that the contrast between different structural portion of the brain (gray matter, white matter and cerebrospinal fluid) was acceptable. In the parcellation procedure, brain cortex was classified into sulcal and gyral cortices based on the values of local mean curvature and average convexity. In cases that the average convexity value was lower than a threshold the voxels were considered as sulcal, otherwise the voxels were assumed as gyral [26].

Subjects divided into two groups called the initial set and the training set. Development and testing the nomenclature rules was performed using the initial set. The training set was utilized for training the designed software for automated labeling. The manually labeled second set of hemispheres was used as a training set to produce a statistical surface based atlas with the aim of automatically labeling new hemispheres. Comparison of automated and manually labeling of the training set was accomplished using the leave-one-out procedure. The results show that the proposed method has an acceptable accuracy in automatically labeling the cortical surface. For instance the areas of the Medial orbital sulcus was $5.60cm^2$ and $5.34cm^2$ for the right and the left hemispheres and the respective CIC (The global

Concordance Index averaged across subjects after boundary correction) were 0.96 and 0.95. One of the positive points of this method is labeling the cortical surface in standard terminology [26].

Given the importance of cortical sulci and gyri in the registration of human brain MR images, the automatic sulci recognition has attracted the attention of many researchers. In the literature, various methods have been recommended for segmentation of sulcal region or sulcal basin. Li et al. [52] researched on the automatic cortical sulcal parcellation and proposed a solution for segmentation of sulcal regions and sulcal basins. The proposed method in this paper was applied to T1 weighted images of normal subjects. They used the geometric characteristics such as principal curvatures and principal directions of cortical surface. First of all, the estimation of two geometric characteristics on the cortical surface was done. The fact that the maximum principal curvatures have different signs in sulcal (negative) and gyral (positive) regions, was the basis of this research [52].

The sulcal region segmentation was achieved by applying the hidden Markov random field model (HMRF) and the expectation maximization (EM) algorithm on the maximum principal curvatures of the cortical surface. Then, the production of a smooth tangent flow field was accomplished by solving a variational equation which diffused the principal direction field. At the end of the procedure, the recognition of sulcal basins was performed by employing of flow field tracking method on the obtained tangent flow field [52].

Visual and quantitative evaluations were employed for the accuracy assessment of the proposed method. By using of simulated T1-weighted MR images combined with different levels of noise, the reproducibility of the proposed method was examined. The results of comparative study showed that the proposed method in this paper has a better performance in comparison to a watersheds based method described in [70].

As regards high accuracy and speed as two requirements of a segmentation method in clinical practice, Ltjnen et al. attempted to optimize a procedure of multi-atlas brain MR images segmentation [56]. Multi-atlas registration consists of three stages:

1. Pre-processing

2. Calculating similarity measures in non-rigid registration

3. Atlas selection

2.4.3 Combining multi-atlas segmentation and intensity modeling

There are several methods for each of the above mentioned stages. Optimization of multi-atlas registration procedure depends on the improvement of these stages. In [56], after intensity normalisation of atlases, registration of atlases and target images was accomplished using a 9-parameter affine transformation. It was demonstrated in the literature that the highest accuracy of multi-atlas segmentation is achieved if an optimal subset of the atlases is selected instead of using all atlases. In [56], five recommended methods for atlas selection were examined.

It is shown that using intensity difference as a similarity measure results in the same segmentation accuracy as the standard NMI[1]-based segmentation, while the time complexity decreases threefold [56]. The results show that the atlas selection method based on NMI after non-rigidly aligning atlases to a target image, is the best method. In [56], two approaches were suggested for combining multi-atlas segmentation and intensity modelling by applying Expectation Maximization and optimization using graph cuts.

Patenaude et al. proposed a model for automatic segmentation of subcortical structures in MR images of the brain [62]. In the suggested method, anatomical training information was provided by labelling the image data manually. They trained the models using manually labelled T1-weighted MR images. The probabilistic relationships between the shape and the intensity of images were considered using the Active Shape and Appearance Models in a Bayesian framework. Moreover, the process of fitting extra empirical scaling parameters which is necessary in standard Active Appearance Models (AAM), was eliminated. The Active Shape Model (ASM) which is a segmentation method for medical images and the AAM

[1]Normalised Mutual Information

is an automated segmentation method which uses intensity information. In other words, the AAM connects the shape and intensity models with a matrix obtained from the training set. The presented method in this research is able to analyse differences between the shapes of different groups and demonstrates the location of the changes [62].

Lohmann et al. presented a method for the detection and imputation of neuroanatomical labels to the sulci [55]. They used image analysis methods and MR images from human brains. The input data included 37 T1-weighted MR images of healthy subjects. After a pre-processing step, an automatic procedure to extract the brain from non-brain tissue was employed [55].

Extracting sulcal basins from MRI images consists of a sequence of image analysis steps. After separating white matter from other tissues, segmentation of white matter was performed using simple thresholding techniques and a region growing algorithm. Then, the automatic labelling of sulcal basins was accomplished using a model matching procedure that uses a point distribution model for describing spatial alternations and also shape similarity measures [55].

The shape and spatial distribution models were matched together for automatically attaching neuroanatomical labels to the sulcal basins. In order to find the best match, a shape similarity measure (Hausdorff distance metric) was used. The reliability and reproducibility of the proposed method for segmentation and labelling have been demonstrated in experiments [55].

There are some available software programs for brain volumetry. Klauschen et al. compared three software packages developed for brain volumetry. They studied segmenters were SPM5 [2], FreeSurfer [23], [30] and FSL [74]. SPM5 implements statistical approaches for analysing neuroimages. FreeSurfer is a brain imaging software package developed for automated surface reconstruction and analysis which calculates measures like cortical thickness, surface area and folding. FSL is a library of image analysis tools for fMRI, MRI and DTI brain imaging data [46].

Functionality of these software packages was evaluated using MR images of brain. This research was designed to answer the two following questions:

1. Which of the above three software packages mentioned is more accurate in

measuring the volume of the gray and white matter of brain?

2. Which of the above three software packages mentioned has sufficient robustness against variation in the quality of MR image?

This research also explored the algorithmic effects on the volumetric variation. The assessment of within-segmenter performance (effect of image quality) was performed by acquired data from Montreal Neurological Institute. The results show that the accuracy of measuring gray and white matter volume was adequate in SPM5 and FSL segmenters. Moreover, the results revealed that the FSL and FreeSurfer methods have the utmost robustness against variation of image quality in measuring white and gray matter, respectively [46].

2.4.4 Brain Tumors Segmentation

Segmentation of brain tumor is important for subsequent clinical treatments. The process consists of discriminating between different aspects of tumor pathology such as solid or active parts, edema, and necrosis from healthy parts such as gray matter and cerebrospinal fluid (CSF) [35]. All these parts are illustrated in Figure 2.3 [22].

For brain tumor segmentation, we have three categories enumerated in the literature by Foo et al. [31], Olabarriga et al. [59], and Yao [94]; namely manual segmentation, semi-automatic segmentation and fully automatic segmentation. The process of an individual drawing the boundaries of tumors and giving different regions of anatomic structures with different labels is referred to as manual segmentation [94]. This method is based on a single 3D image with intensity enhanced using an injected contrast agent [67]. With the development of computer technologies, most of the tasks in manual segmentation could be automated using intelligent algorithms. However, computing the accuracy of the results is still done manually. This integration of manual and automated system in brain segmentation is called semi-automatic segmentation method.

Machine learning and pattern recognition methods can often solve a problem with results that rival that of human experts. In these methods, the algorithms

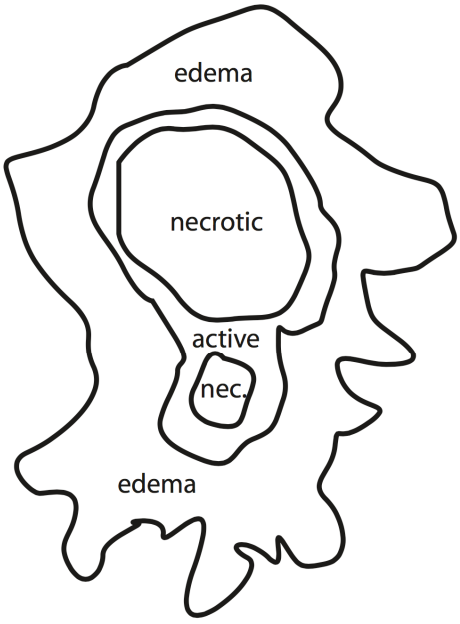

Figure 2.3: Different parts of a tumor [22]

determine the segmentation without any human intervention. In particular, these methods employ prior knowledge and human knowledge in their algorithms [35].

To define the homogeneity of each brain tissue type in brain segmentation, an objective measure is required. There are two ways to achieve this goal, referred to as unsupervised and supervised segmentation methods [72]. Using training data that have been manually labelled is the main difference between unsupervised and supervised segmentation methods.

Wong et al. [89] give three fundamental rules of segmentation; these rules are:

1. Permit quantification which means we should have a model that could describe appearances and also allows variations in appearance

2. Reducing the dataset by focusing on the extracted interested regions during the quantitative analysis

3. Establishing structural correspondences for the physiological data

Based on these guidelines, segmentation techniques are divided into four classes

[94], [28, 63, 89]:

1. Threshold-based techniques
2. Region-based techniques
3. Pixel classification techniques
4. Model-based techniques

The first three classes are commonly employed in 2D image segmentation [9, 44, 50, 86] and the last class is mostly employed in 3D image segmentation [16, 43, 92].

One of the most effective approaches to region segmentation is the threshold-based techniques. These techniques are based on comparing between intensities of the objects in the image with some specified intensity thresholds. Threshold-based techniques are divided into global and local categories. If the histogram of an image is bimodal, the object can be separated from the background of the image by a single global threshold. However, if the image contains more than two types of regions, corresponding to different objects, the segmentation must be carried out using local thresholding [35]. Combining regions of an image by merging neighbour pixels based on a pre-defined similarity criterion is called region-based segmentation [89].

The third class of segmentation methods is based on pixel classification. In this method, the feature space of an image is represented with pixel attributes, which include gray level, local texture and color components [35]. The process of grouping similar pixels into a single cluster, while objects with dissimilar features are grouped into different clusters based on some similarity criteria is called clustering [35]. For clustering pixels in feature space in pixel classification of tumor segmentation, supervised and unsupervised classifiers are used [8]. In particular, fuzzy C-Means (FCM), k-means, and statistical methods such as Markov Random Fields (MRF) and Articial Neural Networks (ANN) are examples of clustering techniques. FCM, k-mean and MRF are used for unsupervised while ANN is used for supervised classifiers [36].

It is not easy to decide whether a pixel belongs to a region or not since the features used for determining homogeneity may not have a sharp transition at region boundaries. FCM is based on concepts of fuzzy set and is a very popular unsupervised image segmentation technique, specifically in brain tumor segmentation [48], [78].

MRF is an unsupervised segmentation method that considers spatial information and the dependency between pixels of the image [81]. Detecting abnormalities of the brain by the multi-layer MRF framework is proposed by Gering et al. [34].

Understanding the rapport between the structure and its function of different parts of the brain is one of the most important goals of neuroscience research which is possible by reducing the anatomical and functional variability among different individuals. The first step uses tools for registration and normalization of provided images of the brain. For example, SPM (Statistical Parametric Mapping) is a package provided for spatial normalization of brain images [82].

Talairach atlas is another tool for detailed description of brain anatomy within the stereotaxic space and is preferred in defining the relationship between the obtained data from functional imaging studies and the Brodmanns areas (BA). However, there are many ambiguities in using Talairach atlas when the position is between different brain areas. For this reason, automatic labeling of brain activations based on the macroscopic anatomical parcellation was proposed. Applying this approach for labeling of brain activation does not remove all ambiguities. Errors caused by these ambiguities affect interpretation of functional imaging studies [82].

Mazoyer et al. performed the process of automated anatomical labeling of detected activations using a macroscopic anatomical parcellation of the NMI single-subject MRI brain template. However, the inter-individual anatomical variability problem is not resolved in this paper. The main purpose of this study is to repress the bewilderment existing in previous works about the anatomical label of a set of coordinates. In this research, T1-weighted gradient echo sequence was utilized and after correction of each acquisition, spatial normalization was performed using a nine-parameter transformation. By segmentation, the average of the acquisitions was divided into eight classes [82].

Automatic anatomical labeling was performed using three procedures including local maximum, extended local maximum and cluster labeling. The local maximum labeling method is widely used in the literature. The weakness of simple local maximum labeling is that it is likely to misplace an activation from one region to its neighbor, as this problem may be seen in the extended local maximum labeling approach [82].

2.5 Skeleton Method

2.5.1 Definition

Medial axis transform has been widely used for extracting new descriptors of shapes and is used in applications such as pattern recognition, object segmentation, registration, and animation [27]. In 2D, the medial axis of a subset bounded by a closed curve is defined as the locus of the centers of all circles each of which is tangent to the curve in at least two points. The constraint is that all the circles are inside the curve [10].

The medial axis transform (MAT) with the associated radius function is a descriptor for shape; in other words, it can be used for reconstructing the original shape. The medial axis concept can be generalized to k-dimensional hypersurfaces by using k-dimensional hyperspheres instead of 2D circles. 3D medial axis is useful for surface reconstruction for physical models [10].

There is a difference between MAT and skeletonization, nonetheless these two concepts are utilized interchangeably. A skeleton is a binary image, while MAT is a graylevel image and the intensity of each skeleton point denotes the shortest distance between the point and the boundary of the original object.

2.5.2 History

The concept of medial axis was proposed in the 60's and several methods can be used to compute it. The medial axis is a method to represent an object for shape analysis and has found applications such as in registration.

Vidal et al. worked in the area with the potential of utilizing skeleton and they

claimed that the skeleton and the medial axis are powerful tools. In their research, they constructed suitable attributed relational graphs (ARG) to arrange information of object shape represented using the medial axis. They also showed how to compare objects from their skeleton-based ARG. Hence, an ARG is a suitable structure for describing the obtained knowledge from an object medial axis [85].

To assess the ability of the skeleton-based ARG matching algorithm, Vidal et al. performed two experiments on object comparison. Three distorted copies were obtained from the original object and then the correspondences between object parts were sought. At the end, ranking of the objects in the series was performed based on the ARG matching outcome [85]. The obtained results show that utilization of a skeleton-based ARG matching allows to get consistent correspondences between parts of an object and it helps to categorize objects based on similarity of shape and topology.

Chan et al. proposed a registration method between 3D magnetic resonance angiographic (MRA) and 2D digital subtraction angiographic (DSA) images [15]. These imaging modalities provide structural information, which is useful for treatments. Multi-modal registration methods are generally divided into two types: feature-based and intensity-based. High accuracy is an advantage of the intensity-based approach. On the other hand, the feature-based method is effective based on the computational aspect. In feature-based registration methods, features such as skeletons, surfaces or curves are extracted in preprocessing steps. Thus, they are faster than intensity-based methods but comparatively less accurate [15] and they usually need some post-processing refinements like the one that is described in our proposed method.

In this paper and in the preprocessing step, an isotropic volume is constructed with the result that the new voxel size is equal to the original in-plane voxel size, and estimation of intensities of voxels between slices was done using trilinear interpolation. A global thresholding method was utilized in vessels segmentation and skeletons were computed using a modified weighted metric. The original volume was recovered by using of skeleton points and the distance transform values [15].

Heretofore certain PDE techniques such as the Hamilton-Jacobi equation have

been utilized to extract medial axis of 2D images. Du and Qin used diffusion equations to extract medial axes of 3D solids represented by polygonal models. Using PDEs to compute medial axis had advantages in modeling geometric objects. PDEs define geometric objects by solving a set of differential equations. The time-dependent diffusion-based equation was solved using finite-difference approximations [27].

Hellier et al. compared the performance of several elastic registration methods on a database of subjects. They concentrated more on the matching of cortical areas than other areas. Global and local measures of the relevance of the registration were used as comparison tools. The method used in segmentation of cortical sulci was based on the active contour paradigm. This paradigm evolved from a 1D curve to a 2D surface models the medial axis of the sulcus. The global measures utilized and demonstrated that the quality of registration depends on the degrees of freedom of the transformation. On the other hand, local measures reveal no noticeable differences between rigid and non-rigid methods [42].

Fritsch et al. applied the multiscale medial axis (MMA) to an image registration task. The authors have shown the possibility of objects description by means of middle/width representations from the intensity distribution of grey-scale images. Pizer et al. in their research proposed a means for characterization of object structure and shape that eliminates the need for an explicit definition of the boundary. Moreover it operates directly from the image-intensity distribution in the object. This method produces a sort of medial-axis description that identifies that axis location and object width must be defined due to a tolerance proportional to the object width [64]. In this paper after a brief presentation of MMA and its computation methods from geometric measurement, some examples of its usage in image registration method and future applications of the MMA were exhibited [32].

Application of MMA in image registration emanates from significant properties of MMA such as figure classification by means of position and width, summarization of the track in the middle of figure and elimination of detailed variations of the object boundary. The authors proposed two methods for image registration using MMA representations that both of them need the user to specify the MMAs of a

reference image [32].

2.5.3 Disadvantages

Applying medial axis to the image has some problems, especially in dealing with a noisy object and in discrete spaces. One of the problems associated with discrete space is the difference between the medial axis and the original topology of the input object. Researchers use discrete homotopic transformations guided and constrained by the medial axis, to acquire homotopic skeleton, which contains the medial axis [66].

The second problem is the instability of medial axis under small perturbations of the original shape. In other words, the medial axis is sensitive to a slight modification of the shape. The importance of this problem is more visible when a small amount of noise is added to the shape. This fact makes clear the importance of filtering which can be applied as demonstrated in the literature. Postolski et al. proposed a new method for Euclidean medial axis filtering. The resulting axes from their proposed method keep significant features of the input object in order to be representative of the shape. So, the proposed algorithm is preferred to other presented methods because of overcoming the shortcomings of other algorithms [66].

Spitzner et al. compared different skeletonization methods and showed that they are sensitive to noise and suffer from instability [77]. Figure 2.4 shows their results. They rotated the image and the results was unstable in terms of the number of joints and branches [77].

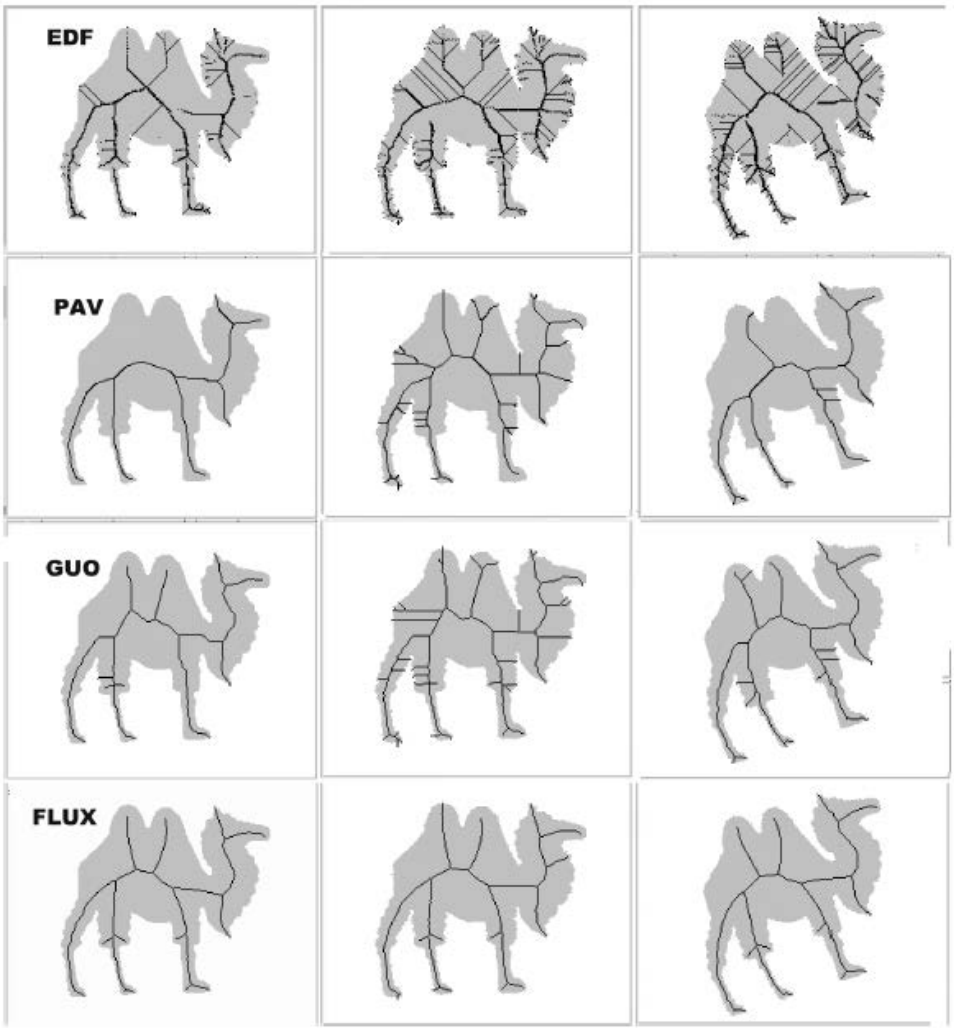

Figure 2.4: Comparison of skeleton results under instability [77]

Chapter 3

Proposed Method

In the previous chapter we reviewed different methods of finding a skeleton of a 2D shape and we investigated their pros and cons. In this chapter a new method to calculate the skeleton of a 2D connected component piece of white matter is presented. The main advantage of this method is that we can find the end points of different regions such as the precentral and postcentral gyri very fast and accurately and it is more robust against different kinds of noise.

Figure 3.1 and Figure 3.2 show the work flow of the new method. Our method consists of the following stages:

- Separate the white matter/grey matter/CSF
- Calculate the skeletons of the left and right hemispheres
- Find the closest subject in the training dataset
- Find the transformation between two skeletons
- Apply the transformation to the labels of subjects image in training data set

3.1 Separating white matter of the brain

The first step of this algorithm is to separate the white matter of the brain from other parts. After separating the white matter we convert it to a binary image which reduces noise and therefore we can recognize the left and right side of the brain more easily. Focusing on the white matter reduces the complexity of the problem, so

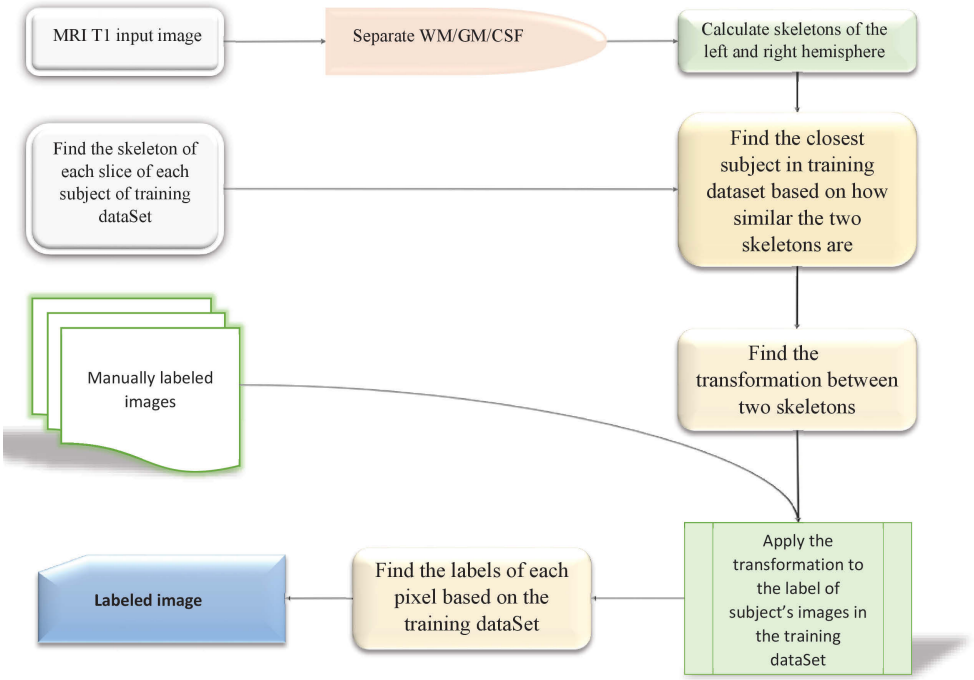

Labeling an MRI T1 image using the proposed skeleton method

Figure 3.1: Work flow of the proposed labling method

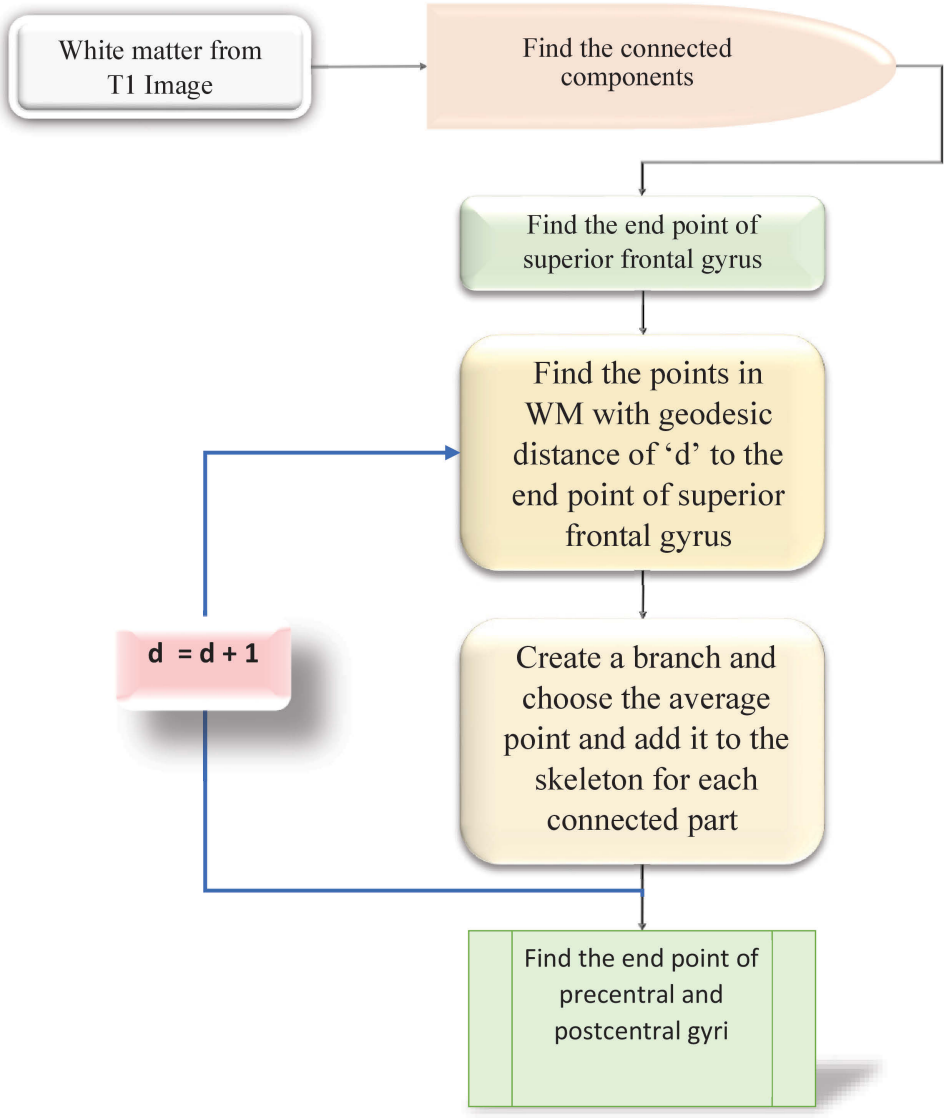

Calculating the skeleton of a white matter image

Figure 3.2: Work flow of the method for generating skeletons

there is no need to map and transform all the voxels. The expectation maximization and other clustering algorithms can separate white matter of the brain very well.

3.2 Calculating the skeleton of the left and right hemisphere

We described several methods in chapter 2 to generate skeleton of a 2D shape. We use the result of skeleton method to find the accurate location of end points of different regions and so the methods described in chapter 2 are not very useful for our problem. Also it is used to calculate a simple representation of white matter so that we can measure how much two skeletons generated from two different images are similar.

The problem with skeleton methods is that they are either not very simple or are very sensitive to noise. You can see the result of the morphological skeleton that is implemented in Matlab environment in Figure 3.3. Our proposed method to find the skeleton has the advantages of being very fast, which is linear in terms of the number of pixels, and also it can represent the shape of white matter (See Figure 3.3). In this section we explain the steps of creating the skeleton in details.

3.2.1 Finding connected components

The results of segmentation algorithms is the probability map of the probability of assigning a pixel to different types of matter. We used a threshold to convert the white matter into a binary image which means we consider a pixel as white matter if and only if the probability of that voxel belonging to white matter is greater than the defined threshold. After that, connected components of slices are calculated by applying a depth-first-search algorithm with 8-connectivity, which means that each pixel is adjacent to its neighbor pixels with a distance of 1, on the 2D slice. Then we sort the connected components by their size and then the two largest components are recognized as the left and right side of the brain. By comparing their coordinates we can distinguish the left side from the right side of the brain.

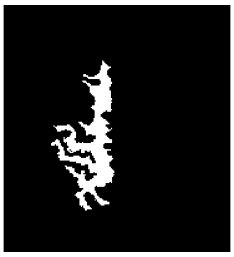

(a) White Matter

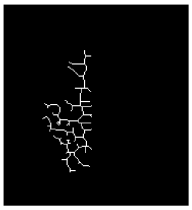

(b) morphological skeleton

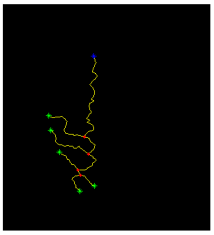

(c) our skeleton method

Figure 3.3: Comparing morphological skeleton method implemented in Matlab with our proposed method

3.2.2 Finding the boundary line between two parts

By considering the two largest connected components and finding the midpoint between them, we can calculate the vertical line that separates the two components. That line between the left and right parts of the brain is obtained by finding the bounding box of the two parts which have been determined previously. By using the two bounding boxes we can easily define the the separating line of the two hemispheres.

Suppose $P = \{(x,y) \,|\, (x,y) \in Component\ 1\}$ is the set of points in the first component and $Q = \{(x,y) \,|\, (x,y) \in Component\ 2\}$ is for the other one. The bounding box of P is defined by four points: $P_0 = (P_{minx}, P_{miny})$, $P_1 = (P_{minx}, P_{maxy})$, $P_2 = (P_{maxx}, P_{miny})$, $P_3 = (P_{maxx}, P_{maxy})$ where

$$\begin{aligned} P_{minx} &= min\{x \,|\, (x,y) \in P\} \\ P_{miny} &= min\{y \,|\, (x,y) \in P\}. \end{aligned} \tag{3.1}$$

Q_0, Q_1, Q_2 and Q_3 are calculated similarly from Q.

The separating line is described by two points P_{midUp} and $P_{midDown}$ which are calculated by Eq. (3.2).

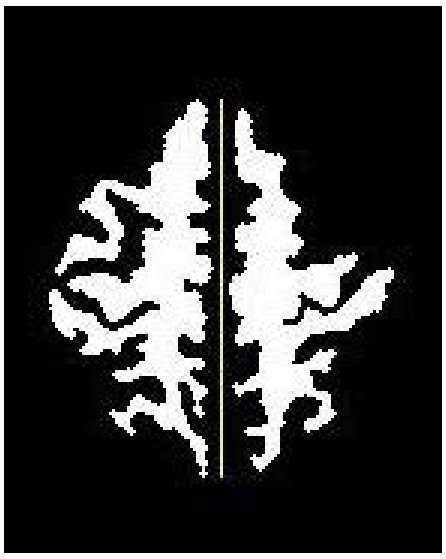

Figure 3.4: The result of section 3.2.2

$$
\begin{aligned}
P_{midUp} &= \begin{cases} (\frac{P_{maxx}+Q_{minx}}{2}, max\{P_{maxy}, Q_{maxy}\}) & \text{if } P_{maxx} < Q_{minx} \\ (\frac{P_{minx}+Q_{maxx}}{2}, max\{P_{maxy}, Q_{maxy}\}) & otherwise \end{cases} \\
P_{midDown} &= \begin{cases} (\frac{P_{maxx}+Q_{minx}}{2}, min\{P_{miny}, Q_{miny}\}) & \text{if } P_{maxx} < Q_{minx} \\ (\frac{P_{minx}+Q_{maxx}}{2}, min\{P_{miny}, Q_{miny}\}) & otherwise \end{cases}
\end{aligned} \tag{3.2}
$$

Figure 3.4 shows the output of this stage. This information can be used to determine the left and the right side automatically.

3.2.3 Creating a connectivity graph for white matter

Component detection is performed by a depth-first-search algorithm. For each side of the brain, a connectivity graph is constructed. A graph is represented by its vertices and edges. In our case the vertices are white matter pixels and two vertices are adjacent if and only if their distance is less than $\sqrt{2}$. By using the constructed graph, it is possible to find the connected components very efficiently. Two pixels are considered in the same component if and only if they are connected by a path in the graph. To avoid noise, a morphological filter is applied to the image to remove sharp edges on corners.

To calculate the skeleton with this method we need to define a starting point. We assume that the endpoint of the superior frontal gyrus is the top most pixel of

the connected component. Our analysis on all of the MRI T1 images taken from 20 subjects shows that this assumption is valid.

The algorithm starts with the starting point as the root of a tree and at iteration d we explore every pixel which has a geodesic distance of d to the starting point. These points form a set of connected curves. For each connected curve we calculate the mean coordinates of its pixels. In particular, define $N(d) = \{(x, y) \mid (x, y) \in P \; and \; dist_{geodesic}(x, y) = d\}$ to be the pixels with geodesic distance d to the root. $N(d)$ could be partitioned into one or several disjoint connected curves as shown in Eq. (3.3) where $N_i(d)$ is a maximal set of pixels that are connected which means N_i are disjoint sets. Then for each curve we calculate the average of its pixels $c_i = mean(N_i(d))$. These nodes are added to the skeleton and their parent is set to their corresponding node in skeleton with distance of $d - 1$.

$$N(d) = \cup_{i=1}^{k} N_i(d) \tag{3.3}$$

When there is more than one connected component, e.g. in Eq. (3.3) $k > 1$, we will have a branch at this point by adding a node to each individual connected component. Figure 3.5 shows a situation when a branching occurs. The distance of blue pixels are the same from the initial point. The red pixels are the mean of each connected curve. We continue these iterations until every pixel has been reached. The resulting tree may still have some unwanted nodes that do not represent the skeleton properly. To overcome this problem we prune the tree by using some simple rules.

3.2.4 Pruning the tree

In order to prune the constructed tree, we eliminate areas which are not large enough. In particular, areas less than 20 pixels are removed. Each pixel in the graph is corresponded to a specific node in our tree. Then we merge remaining pixels to the parent node of their corresponding node in the tree. After some iteration the tree is completely pruned and small or large artifacts due to noises are easily removed . By definition of leaf nodes in a tree, the endpoints of each region would be one of them.

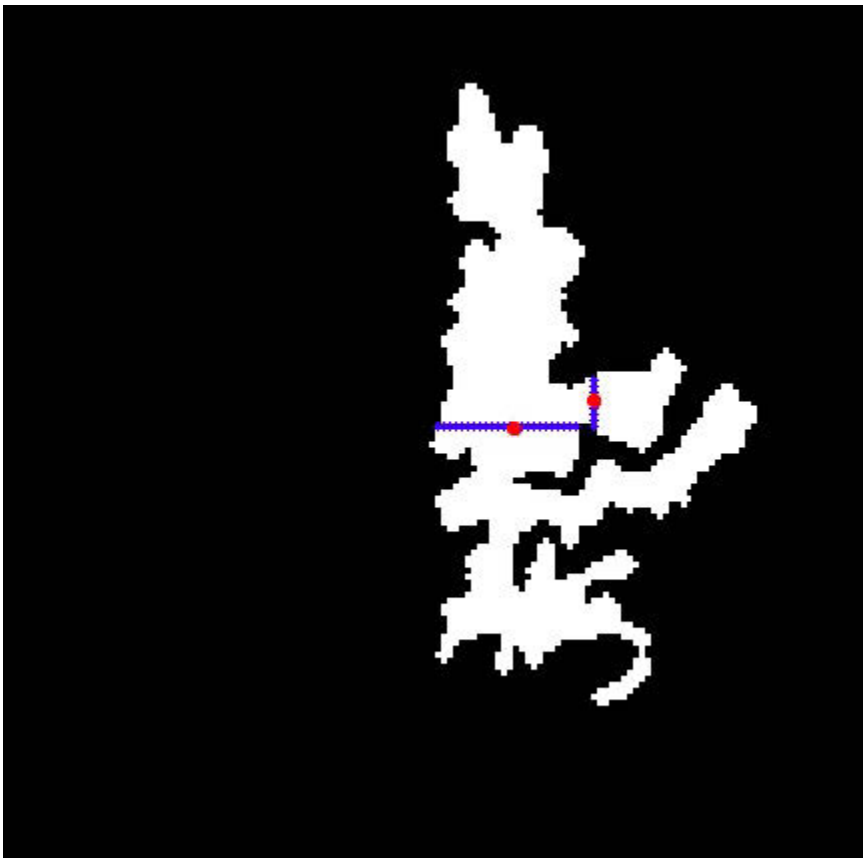

Figure 3.5: A branch in skeleton. Blue pixels have the same distance to the initial point. Red pixels are the average of each connected curve.

Also if the difference of depth of a node from depth of its branching ancestor is less than a threshold we eliminate that branch including the node itself. The branching ancestor is one of the ancestors of that node with more than one children. We used 10 for the threshold in this thesis.

3.2.5 Creating the Skeleton

After completing the previous steps, we have the skeleton which is represented by a tree for both the left and right side of the brain. However, this skeleton is not smooth enough and so the goal has not been accomplished yet which is a skeleton robust to noise.

The skeleton is going to represent the shape of white matter and we use it to find the best registration between the input image and our images in the training data set. Our experiments in chapter 4 shows that calculating the transformation between two skeletons is more robust to noise compare to calculating the transformation using image intensities even by using all of the 3D voxels. The reason is that the skeleton can represent the shape and structures of white matter and is simpler because it has much fewer points. The first output of the extracted skeleton is shown in Figure 3.6. The yellow points are the skeleton and the red points shows the branching in the skeleton.

Calculating the skeleton is done by starting from the top point of superior frontal and finding the nodes that are adjacent to the previous layer. The average of coordinates of pixels in the next depth produces another point in the skeleton tree. Each of these points is considered as a vertex in the tree. For calculating the structure of the skeleton, first a breadth first search algorithm is performed on the graph to find the depth of each point. We assume that the top most pixel in the superior frontal component is the initial vertex and the depth of that pixel is zero. We use two features of nodes to determine the endpoints of the precentral and the postcentral gyri. The first one is the geodesic distance of that node to its branching ancestor. The other one is their coordinates which are determined by a threshold learned from a set of training data set. These points are shown in Figure 3.7.

The skeleton represents the shape and curvature of the white matter. With this

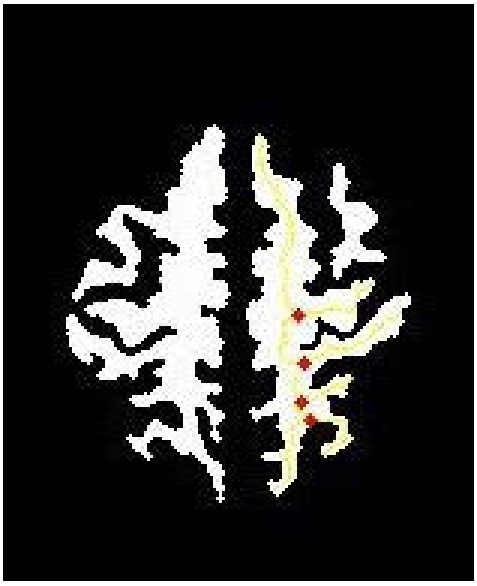

Figure 3.6: The result of section 3.2.5

representation we can register one image of a subject to another MRI T1 image. To achieve this goal we should first calculate the transformation that registers the first image to the other one. As discussed in the previous chapter, there are different types of transformations with different degrees of freedoms. For the proposed method we use affine transformation which has 12 degrees of freedom. The advantage of using this transformation is that we can calculate the transformation very efficiently and our studies show that with this transformation we get encouraging results. The next section will discuss the details of how the transformation is calculated.

3.3 Find the closest subject in training dataset

Now we explain how we choose the best image from the set of training dataset to calculate the best transformation that registers the input image to the other one.

In the previous section, we presented a method to calculate the end points of four regions by looking at the leaf nodes of the skeleton. To find the best affine transformation, we need to have enough corresponding points, i.e. at least three, between two images. The end points of all four regions are located with high accu-

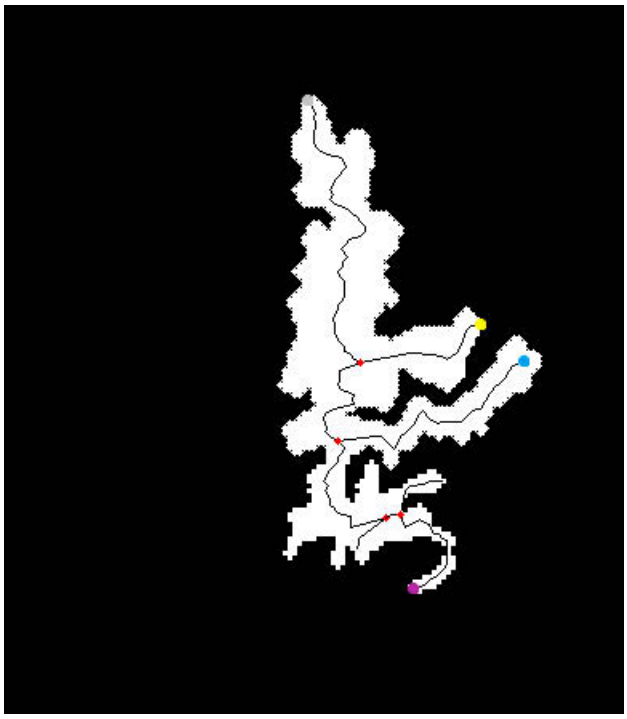

Figure 3.7: Calculating skeleton for the right side of the brain. The endpoints of precentral (yellow dot) and postcentral gyri (blue dot) is specified in the skeleton.

racy, but we need more points to make the resulting transformation robust to noise. For this reason we need additional points.

For this purpose we use sampling on parts of the skeleton that connects the precentral gyrus to the superior frontal and the one that connects the postcentral gyrus to the superior parietal lobule. We chose these two curves to make the resulting transformation more robust to shape variations. Since the skeleton is represented by a set of nodes, we cannot simply sample points on the skeleton because there is no guarantee that the distance between any two nodes on the skeleton are the same in every subject brain image. To overcome this issue, we fit a curve that represents the corresponding part of the skeleton so that when we traverse a certain length on one curve, we traverse the same length on its corresponding curve on the other subject. Figure 3.8 shows the curve between superior frontal endpoint and postcentral endpoint for two subjects. We uniformly sample from these curves to get the sufficient points to find the transformation between two skeletons.

To find such a curve we fit a cubic smoothing spline on nodes uniformly sampled

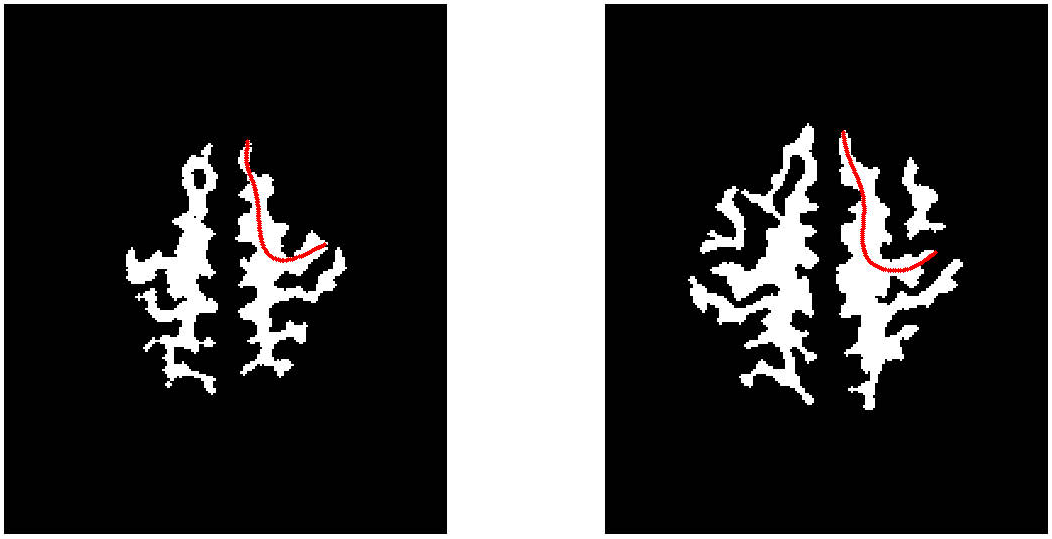

Figure 3.8: Sampling points on the curve between superior frontal endpoint and pretcentral endpoint

from the skeleton. It should be taken into account that the uniformed samples from the skeleton does not preserve distance homogeneity but when we fit a spline on the sampled nodes, the spline itself does preserve the distance homogeneity.

$$p \sum_{j=1}^{n} \omega(j) \mid y(j) - f(x(j)) \mid^2 + (1-p) \int \lambda(t) \mid D^2 f(t) \mid^2 dt \qquad (3.4)$$

In other words, the spline f is calculated by minimizing Eq. (3.4) where p is the smoothness parameter, ω is the error measure which depends on the point, $y(j)$ is the values of data at points $x(j)$, λ is the roughness measure weight function which we set it to 1, $D^2 f$ denotes the second derivative of f and the integral is over the smallest interval containing all of the entries of x [24]. We used $p = 0.9$ and set ω to be a uniform distribution in this thesis. $f(.)$ is a 2-dimensional function that we want to estimate and $y(j)$ is our j_{th} 2D data point. We used the implementation in Matlab environment to solve the equation in this thesis.

By obtaining the spline, we can sample any required number of points to perform the next step. After sampling points from the skeleton, we would have enough data to find the best affine or more complex transformations to find the best tranformation that registers two skeletons into same space. If we compare this method to

other methods that use the whole image to find the best transformation, we could see that since we use much fewer number of points, the whole process is much faster.

3.3.1 Finding the transformation between two skeletons

In this section, we explain the mapping procedure between two skeletons. The extracted points from the previous step are used for this step. Consider P_0 as the set of points in the destination image and P_1 as the set of points in source image. We used 100 points in this thesis. The goal is to calculate the transformation V in Eq. (3.5) where V is a 3×3 matrix, P_0 and P_1 are two $2 \times N$ matrices where N is the number of points. If the label of the training image is L_1 we can obtain the labels of destination image very similar to Eq. (3.5) by replacing P_0 by L_0 (labels of destination image) and P_1 by L_1 (source image). The affine transformation is calculated by optimizing Eq. (3.5) using mean squared error (MSE) estimator.

$$\begin{pmatrix} P_0 \\ 1 \end{pmatrix} = V \begin{pmatrix} P_1 \\ 1 \end{pmatrix} \tag{3.5}$$

3.3.2 Applying the transformation to the labels of source image

After obtaining the transformation that registers the skeleton of the source image to the destination image, we apply the same transformation as an initial estimate of the label of the corresponding pixel map to the label of each pixel in the destination image. Eq. (3.6) denotes how the initial values for labels are obtained.

$$label_{destination}(u, v) = label_{source}([x, y] \times T^{-1}). \tag{3.6}$$

3.4 Refine estimation

After performing the previous steps we have obtained an estimation of labels of each pixel of the input image but the result is not acceptable yet because of some noise or inhomogeneity of labels. To refine our results we applied another optimization to enforce a smoothness constraint on the labels using graph cuts. Figure 3.9

shows the results before and after this step.

3.4.1 Graph cuts optimization

Graph cuts has been used in many optimization-based algorithms in computer science applications. The goal is to find values of a function by minimizing an energy function which consists of a data term and a smoothness term. Eq. (3.7) denotes the minimization problem,

$$E(L) = \sum_{i=1}^{n} E_d(X_i, L(X_i)) + \alpha \sum_{u,v \in N} E_s(L(X_u), L(X_u)), \tag{3.7}$$

where α determines the smoothness parameter, E_d is the cost of labeling each node and E_s is the smoothness energy function which determines the cost of labeling two neighbors X_u and X_v differently. N is the neighbourhood of nodes in graph.

For our problem we used the estimation obtained from the previous steps described in section 3.3.2 for E_d. For the smoothness term we set $\alpha = 1$ and used 8 connectivity neighborhood for each adjacent pixels in the connected component as shown in Eq. (3.8). For our experiments we set $c_1 = c_2 = c_3 = 100$. Figure 3.9 compares the final result on one subject before and after refinement. The results for more subjects can be found in chapter 4.

$$E_s(l_1, l_2) = \begin{cases} 0 & \text{if } l_1 = l_2 \\ c_1 & \text{if } l_1 = precentral \text{ and } l_2 = postcentral \\ c_2 & \text{if } l_1 = prececntral \text{ and } l_2 = superiorfrontal \\ c_3 & \text{if } l_1 = postcecntral \text{ and } l_2 = superiorparietallobule \\ \infty & \text{otherwise} \end{cases} \tag{3.8}$$

3.5 Conclusion

In this chapter we present a new method to register and segment white matter of a single slice of an MRI T1 image of the brain. First, we used current segmentation methods to separate white matter from other parts of the MRI image. Then we give a new method to find the skeleton of white matter for a single slice. Then, we

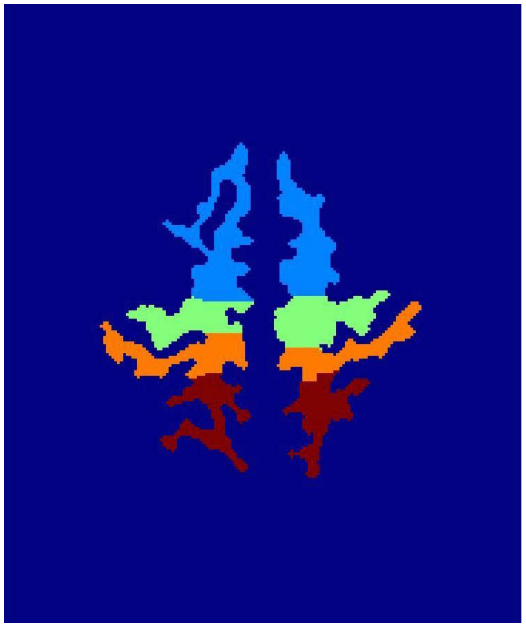

(a) ground truth

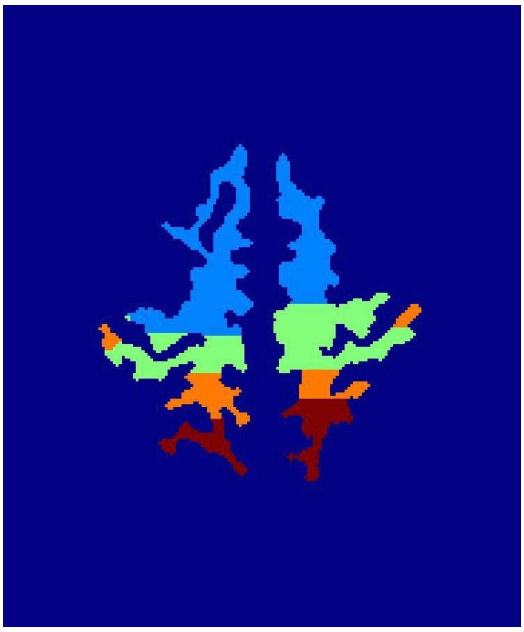

(b) before refinement

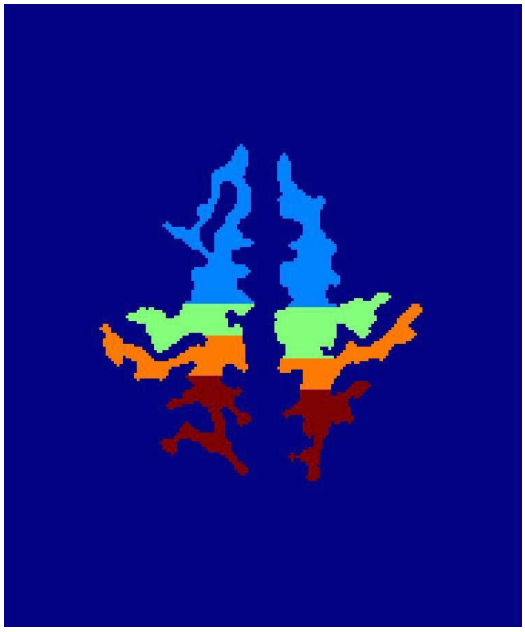

(c) after refinement

Figure 3.9: The effects of refine estimation on subject 1

compared the obtained skeleton to other pre-calculated skeletons from our dataset to pick the best one that is most similar to the skeleton of input image. Then we calculated the best transformation that registers the input image into the chosen image's space efficiently. This gives us an estimation of labels for each pixel. In the final step we applied graph cuts optimization to refine the results.

Chapter 4

Experimental Results

In this section, we present and analyze the experiments which have been done using the proposed method and also compare them with the results reported by ART[1], one of the best methods for automatic detection, segmentation and registration of different parts of the brain.

At first, the data set which has been utilized in this project is introduced. Then, the definition of the performance measurements is given. The next part of this chapter is on system specification, time and memory complexities of our method. Finally, a comparison and analysis with different methods is presented.

4.1 Dataset

There are several MRI T1 datasets that are manually labeled by scientists. However, all of them considered white matter as a single region except the one presented in [37]. Therefore, we use this dataset only for evaluating the proposed method and comparing the results with that of using other state of the art methods.

As mentioned above, the dataset which was provided by Hammers et al., 2003 [37] is used in this work. They studied 20 normal subjects (10 women and 10 men; median age 31 years) with high-resolution magnetic resonance imaging (MRI) scanning. Images were nonuniformity corrected and reoriented along both the anterior-posterior commissure (ACPC) line horizontally and the midsagittal plane sagittally.

[1] Automatic Registration Toolbox

They also studied 20 healthy volunteers from the database at the National Society for Epilepsys MRI Unit. Theses volunteers had no neurological, medical, or psychiatric condition and normal MRI studies as determined by two experienced neuroradiologists. In this dataset, there were 10 women (median age 30.5 years, mean $\pm SD$ 31.6 ± 9.9 years) and 10 men (median age 30.5 years, mean $\pm SD$ 31.5 ± 9.5 years) [37].

4.1.1 MRI acquisition

MRI scans were obtained on the 1.5 Tesla GE Signa Echospeed scanner at the National Society for Epilepsy. A coronal T1 weighted 3D volume was acquired using an inversion recovery prepared fast spoiled gradient recall sequence (GE), $TE/TR/NEX$ = 4.2 msec (fat and water in phase)/15.5 msec/1, time of inversion (TI) = 450 msec, flip angle = 20, to obtain 124 slices each of 1.5 mm thickness with a field of view of 18 $\times$ 24 cm with a 192 $\times$ 256 matrix. This covers the whole brain with a voxel size of 0.9375 $\times$ 0.9375 $\times$ 1.5 mm. The normalized images were resampled with isotropic voxel sizes of 1 $\times$ 1 $\times$ 1 mm^3 in a matrix of x/y/z dimensions of 182/218/182 voxels [37].

As mentioned in the previous chapter, we use only the white matter part of the brain. So, in our method, for each of the 20 MRI images, we first determine the white matter of the brain and then the other stages of the proposed method are summarized in a block diagram shown in Figure 3.1. For the results in ART we used the original brain image.

4.2 Performance Measures

We report three evaluation measures to show the performance of the new method. These measures are:

1. Area Overlap (Accuracy)

2. False Positives

3. False Negatives

4.2.1 Area Overlap

For comparing registered image and target image we used area and surface overlap. One of the area overlap measurements is target overlap (TO) which is the intersection between two labeled regions, s, in the source image (S) and T_r in target image (T) divided by T_r the area of the region in T:

$$TO_r = \frac{|S_r \cap T_r|}{|T_r|} \tag{4.1}$$

where $|.|$ indicates the area computed as the number of pixels [47] We use Target Overlap as a measure of sensitivity. A summation over a set of multiple regions gives us the total overlap agreement measure for a given registration:

$$TO = \frac{\sum_r |S_r \cap T_r|}{\sum_r |T_r|}. \tag{4.2}$$

This measure is between 0 and 1 and the larger the value for TO the better is the result.

Overlap with the registration output calculated for each brain image is the mean value of area overlap on brain slices of images. The area overlap output for the ART method and the skeleton method is shown in Figure 4.1. It can be seen that the results of the proposed method are better than the results of segmentation of the ART method for every subject. Also, the results of the ART method is consistent with the results reported in [47] in which it evaluates different registration and segmentation methods.

The area overlap of the ART method is very high for some regions but the reason is that the ART method overestimates those regions which lead to very poor accuracy for other parts of the brain. But the accuracy of proposed method is overall higher for all regions.

The reason that our result for the superior parietal lobule for one of the subjects in the left side of the brain is not very good is because the size of that region is very small for some slices and our algorithm labels that region as precentral gyrus but the overall accuracy of other regions is very good.

In Figure 4.2 and Figure 4.3, the area overlap measurements for each segment of brain in the left and right sides of the brain as superior frontal, superior parietal, post central and pre central gyri are shown for both the ART and the proposed methods.

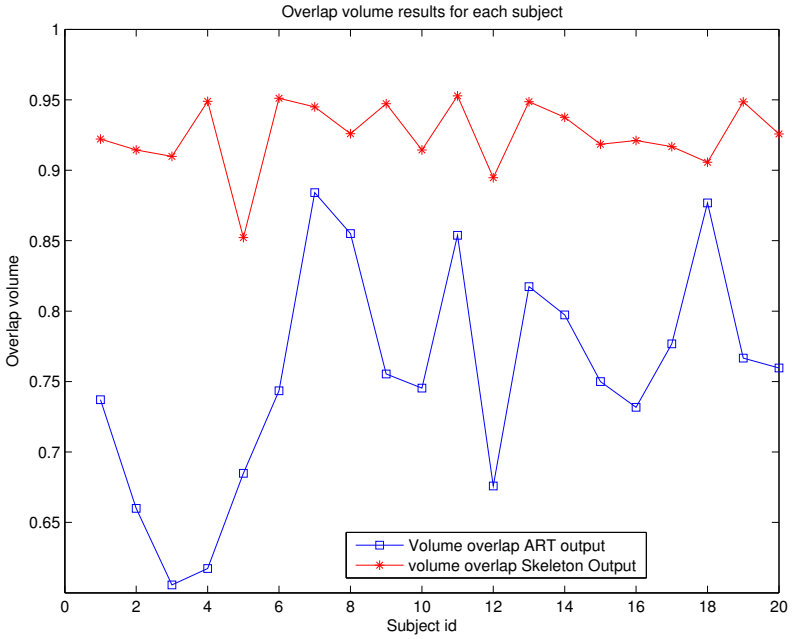

Figure 4.1: Area overlap comparison between ART and the proposed method

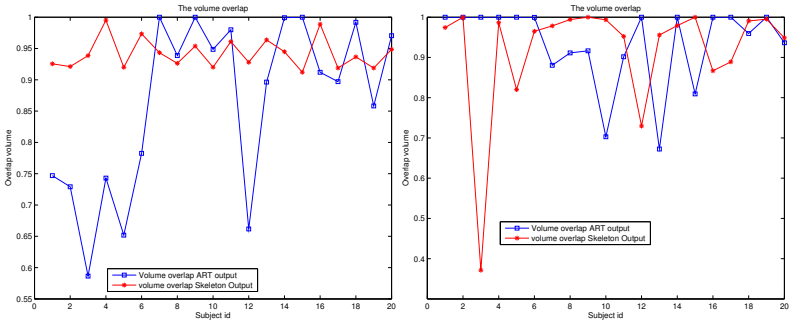

(a) superior frontal (b) superior parietal

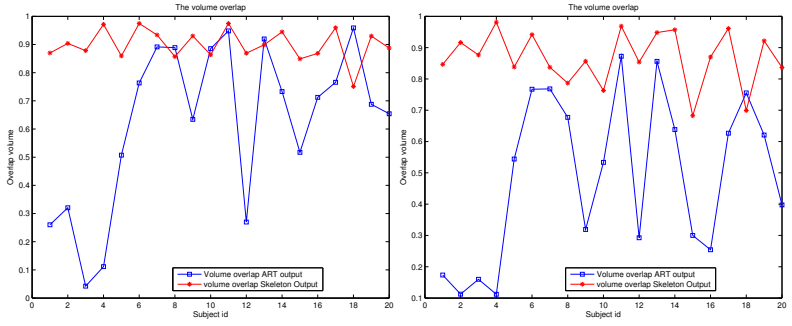

(c) post central (d) pre central

Figure 4.2: The area overlap for the left part of the brain.

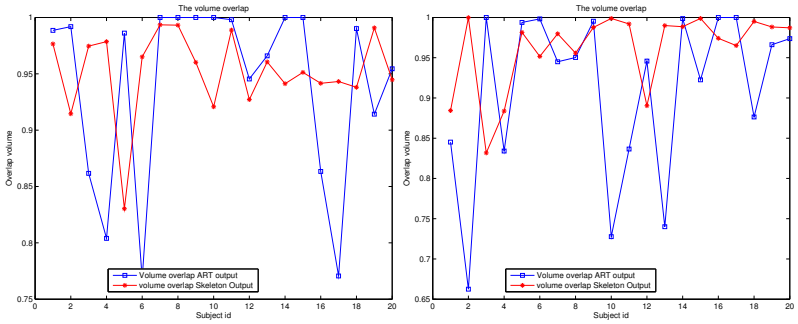

(a) superior frontal (b) superior parietal

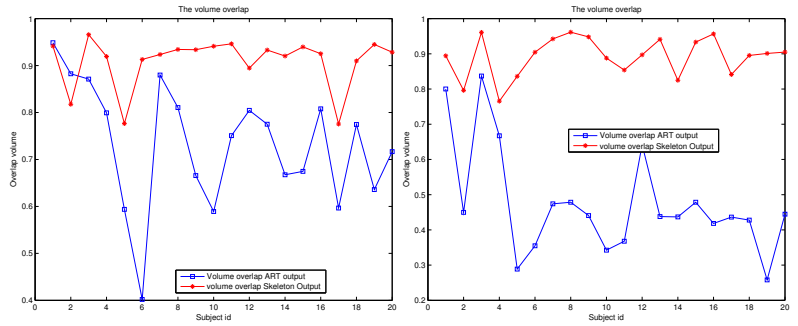

(c) post central (d) pre central

Figure 4.3: The area overlap for the right part of the brain.

The results show the outstanding performance of our skeleton-based method over the 3D registration method, ART.

4.2.2 False Positive and False Negative

We also calculated the false negative (FN) and false positive (FP) errors for the proposed skeleton method. For these errors we characterize the source as a tentative set of labels for the target, and again assume that the target's manual labels are correct. These error measures can range from zero to one; the smaller the error the better the overlap.

A false negative error for a given region is the measure of how much of that region is labeled incorrectly. It is calculated as the area of a target region outside the corresponding source region divided by the area of the target region. As before, it is computed in voxels and summed over a set of multiple labeled regions each

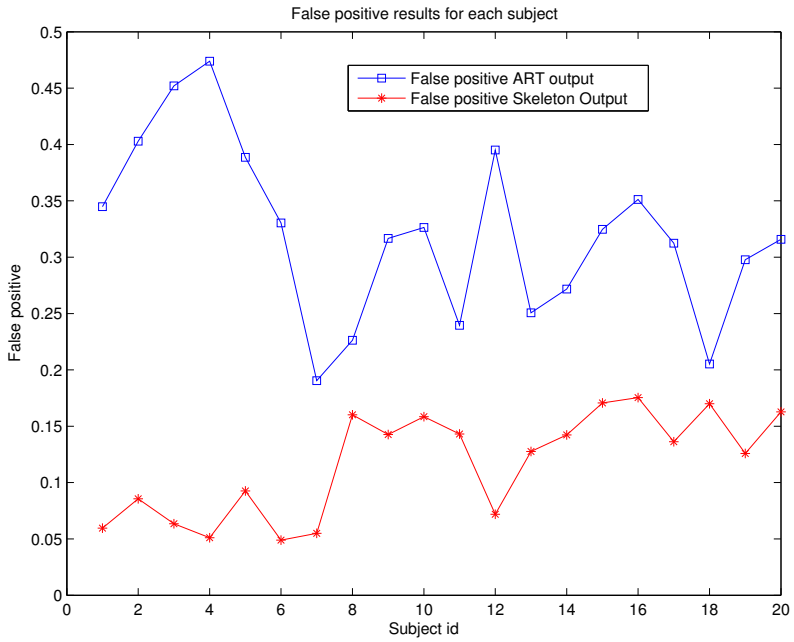

Figure 4.4: The mean of false positive errors of all the subjects.

with index r:

$$FN = \frac{\sum_r |T_r \setminus S_r|}{\sum_r |T_r|}, \tag{4.3}$$

where $T_r \setminus S_r$ indicates the set (theoretic complement) of elements in T_r but not in S_r.

A false positive error for a given region is the measure of how much of the area outside that region is incorrectly assigned the region's label. It is computed as the area of a source region outside the corresponding target region divided by the area of the source region:

$$FP = \frac{\sum_r |S_r \setminus T_r|}{\sum_r |S_r|}, \tag{4.4}$$

where $S_r \setminus T_r$ indicates the set (theoretic complement) of elements in S_r but not in T_r.

Comparison of false positive between the ART method and the skeleton output for each image is shown in Figure 4.4.

False positive measurements for each segment of the brain in the left and right side of the brain as superior frontal, superior parietal, post central and pre central gyri are shown for both methods in Figure 4.5 and Figure 4.6.

Subject	1	2	3	4	5	6	7	8	9	10	11	12	13	14	15	16	17	18	19	20
ART	0.332	0.313	0.332	0.322	0.332	0.313	0.343	0.332	0.322	0.343	0.322	0.325	0.304	0.322	0.322	0.322	0.332	0.336	0.313	0.331
Skeleton	0.06	0.063	0.06	0.059	0.06	0.063	0.048	0.06	0.059	0.048	0.059	0.057	0.064	0.059	0.059	0.059	0.06	0.051	0.063	0.061

Table 4.1: False positive error for each subject (skeleton vs ART).

Subject	1	2	3	4	5	6	7	8	9	10	11	12	13	14	15	16	17	18	19	20
ART	0.472	0.439	0.472	0.454	0.472	0.439	0.488	0.472	0.454	0.488	0.454	0.463	0.426	0.454	0.454	0.454	0.472	0.48	0.439	0.455
Skeleton	0.078	0.078	0.078	0.075	0.078	0.078	0.072	0.078	0.075	0.072	0.075	0.072	0.078	0.075	0.075	0.075	0.078	0.072	0.078	0.072

Table 4.2: False negative error for each subject (skeleton vs ART).

Subject	1	2	3	4	5	6	7	8	9	10	11	12	13	14	15	16	17	18	19	20
ART	0.737	0.712	0.736	0.721	0.738	0.710	0.720	0.737	0.723	0.722	0.721	0.717	0.709	0.719	0.723	0.724	0.734	0.726	0.713	0.725
Skeleton	0.922	0.921	0.923	0.925	0.922	0.923	0.928	0.922	0.925	0.927	0.926	0.924	0.922	0.926	0.924	0.925	0.921	0.927	0.920	0.925

Table 4.3: Volume overlap for each subject (skeleton vs ART).

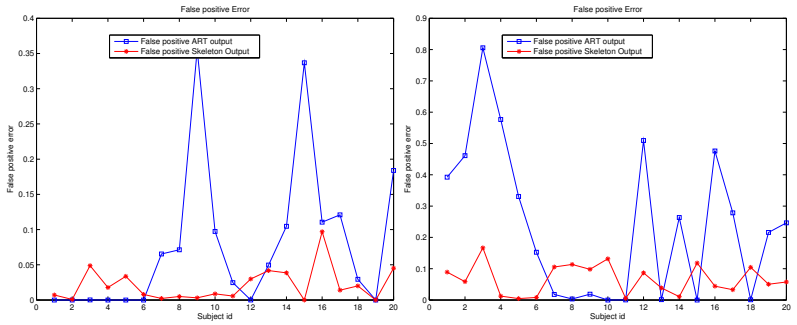

(a) superior frontal

(b) superior parietal

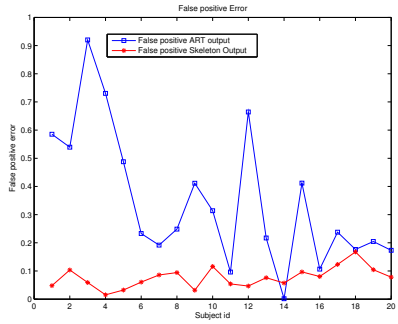

(c) post central

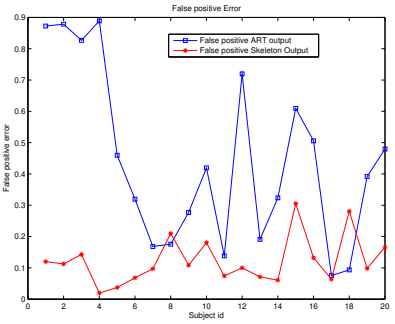

(d) pre central

Figure 4.5: False positive errors of the left part of the brain.

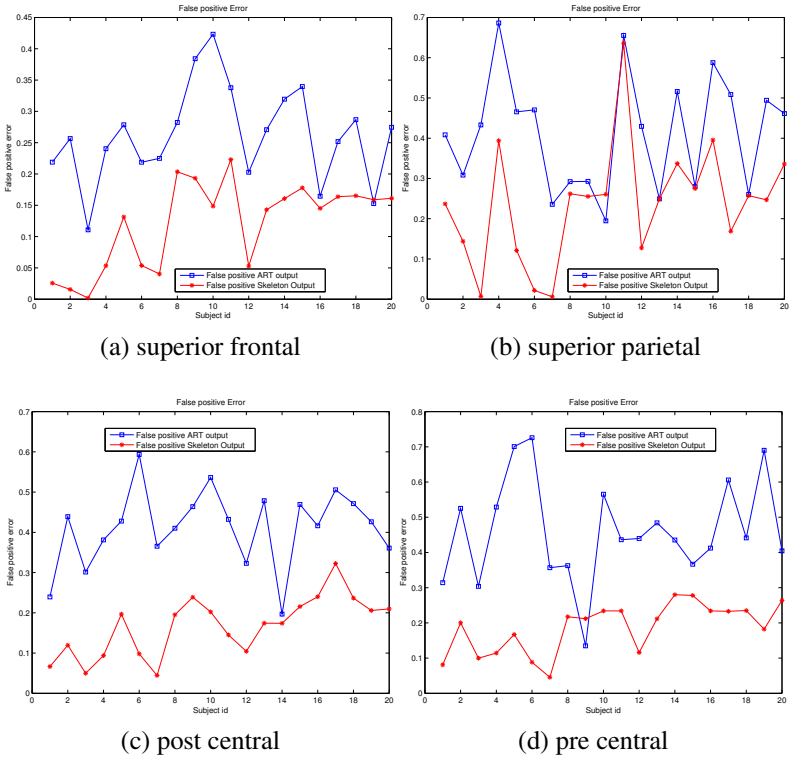

(a) superior frontal (b) superior parietal

(c) post central (d) pre central

Figure 4.6: False positive errors of the right part of the brain.

Comparing of false negatives between the ART method and the skeleton output for each image is shown in Figure 4.7.

False negative errors for each segments of the brain in the left and right side of the brain as superior frontal, superior parietal, post central and pre central gyri are shown for both the ART and skeleton methods in Figure 4.8 and Figure 4.9.

4.2.3 Results for Some Subjects, Before and After Refining Estimation

As mentioned in 3.4, refine estimation is an important step of our proposed method. One of the most important effects of doing this step is to find the largest connected components of the graph created on segments of the brain. Figure 4.10 shows the impact of this step on finding the best segmentation.

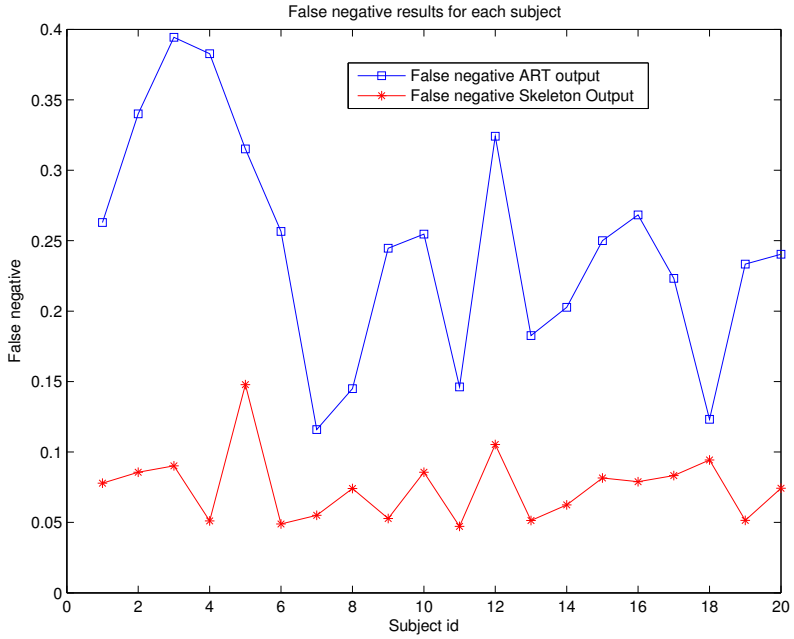

Figure 4.7: The mean of false negative errors of all subjects.

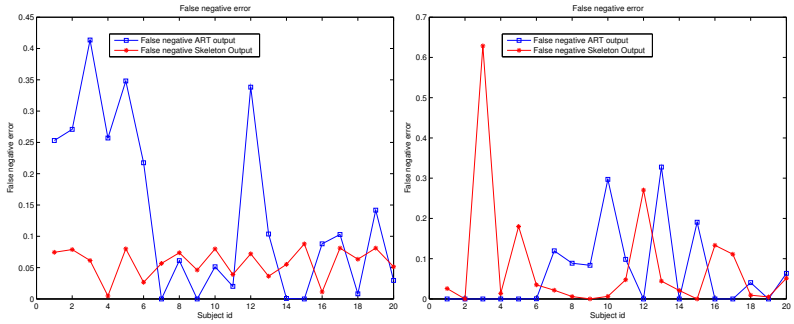

(a) superior frontal

(b) superior parietal

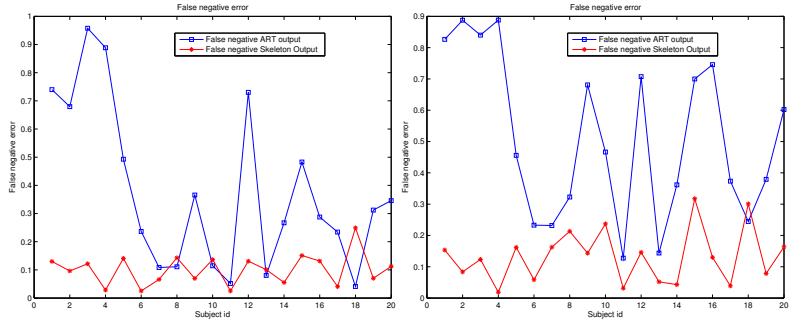

(c) post central

(d) pre central

Figure 4.8: False negative errors for the left part of the brain.

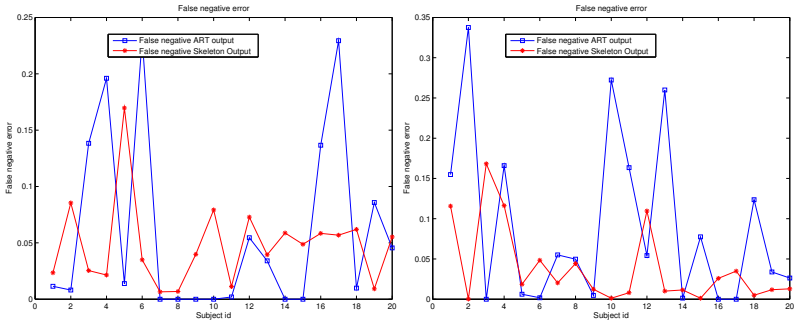

(a) superior frontal (b) superior parietal

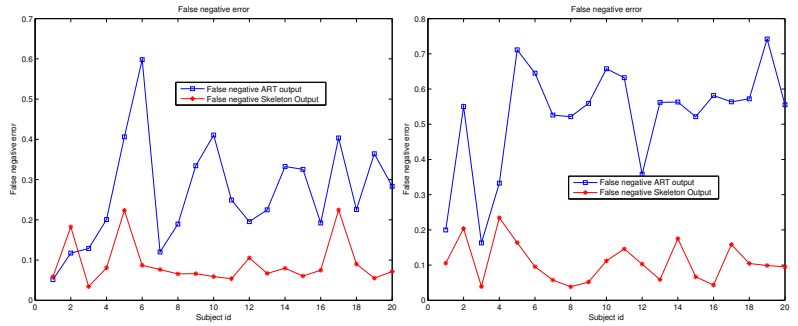

(c) post central (d) pre central

Figure 4.9: False negative errors for the right part of the brain.

Method	Running Time (sec)
Skeleton	21.241
ART	977.054

Table 4.4: Running time comparison between skeleton and ART.

4.3 Time Complexity and Running Time

In this section, a comparison between the proposed method and ART regarding to Time Complexity and Running Time of the algorithms has been proposed.

4.3.1 Running Time

All algorithms ran on a Linux (Mint) system (CPU: Intel Core(TM)2 Due 2667 MHz, 4GB RAM, Graphic: GT218M). All of our codes are written in Matlab environment and programming language and the ART is implemented in C++. Table 4.4 shows the results of running time of two algorithm on this system:

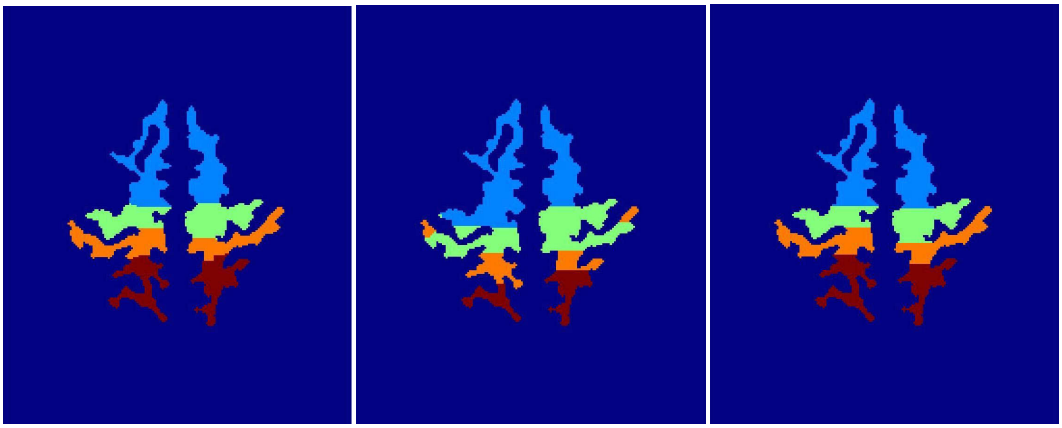

(a) ground truth (b) before refinement (c) after refinement

subject1

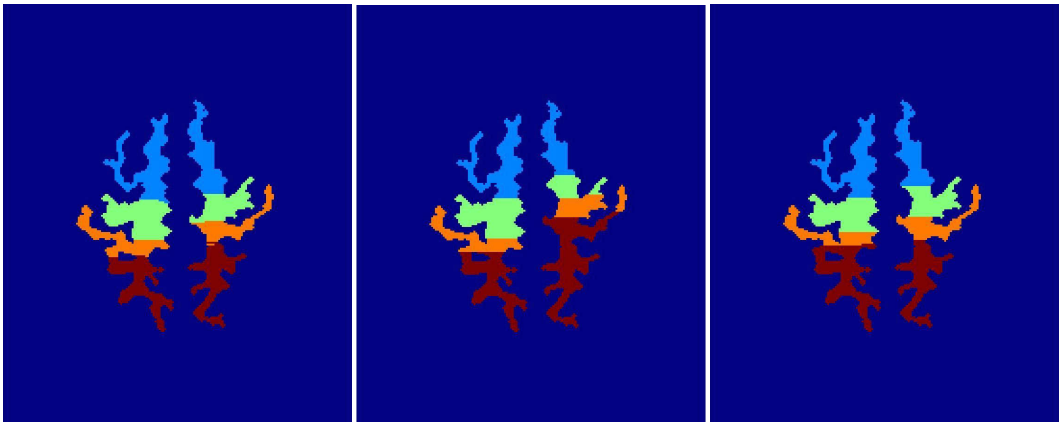

(d) ground truth (e) before refinement (f) after refinement

subject2

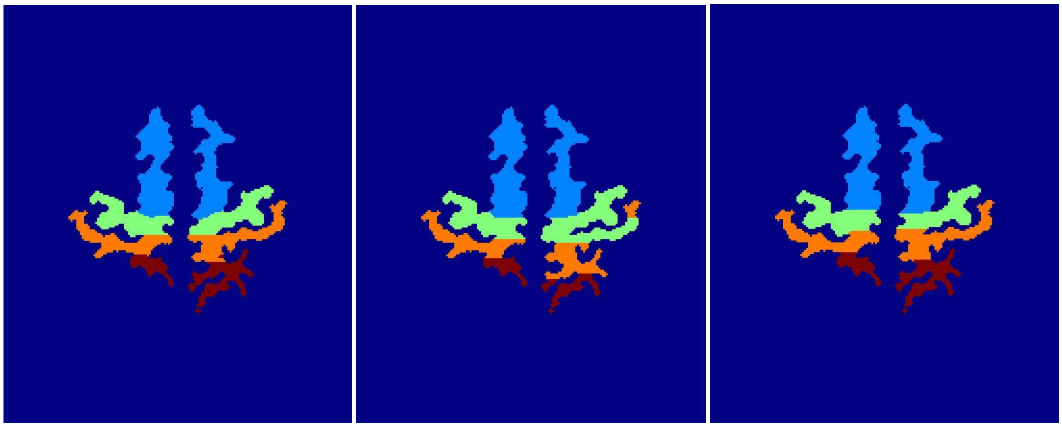

(g) ground truth (h) before refinement (i) after refinement

subject3

Figure 4.10: The effects of refine estimation for subjects 1-9 (slice 127)*(continued)*

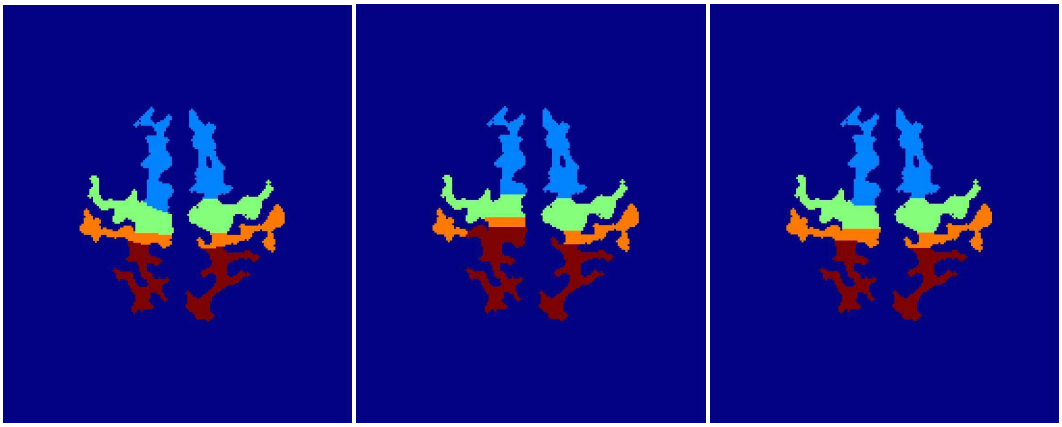

(a) ground truth (b) before refinement (c) after refinement

subject4

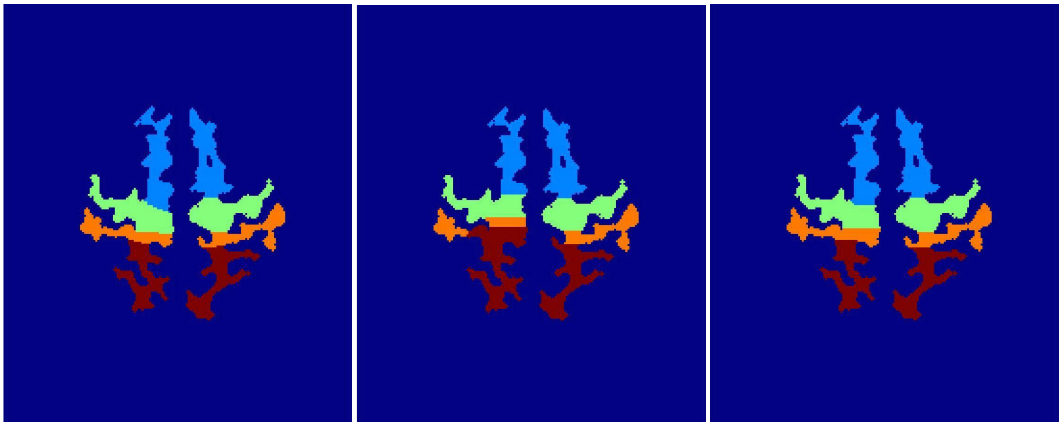

(d) ground truth (e) before refinement (f) after refinement

subject5

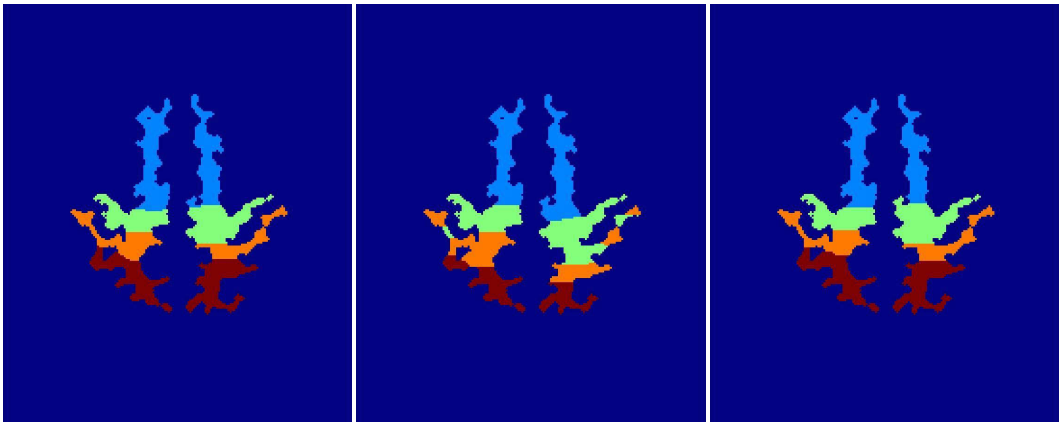

(g) ground truth (h) before refinement (i) after refinement

subject6

The effects of refine estimation for subjects 1-9 (slice 127)*(continued)*

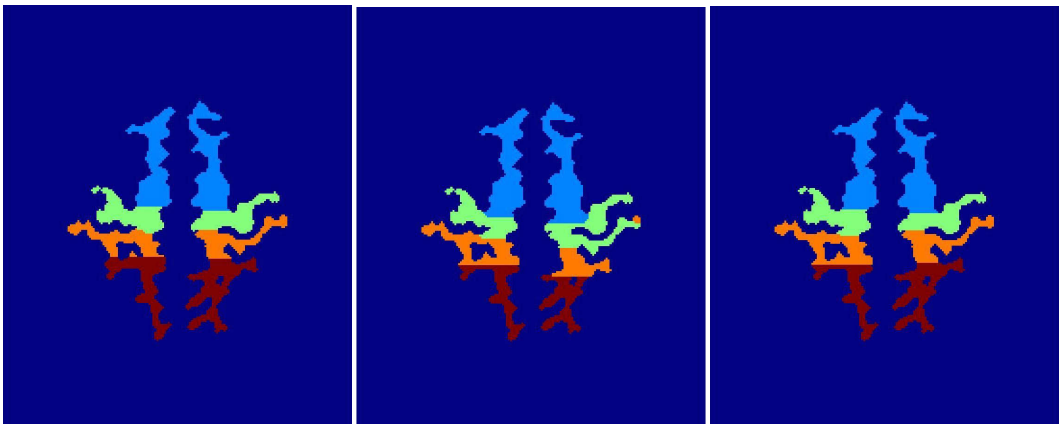

(a) ground truth (b) before refinement (c) after refinement

subject7

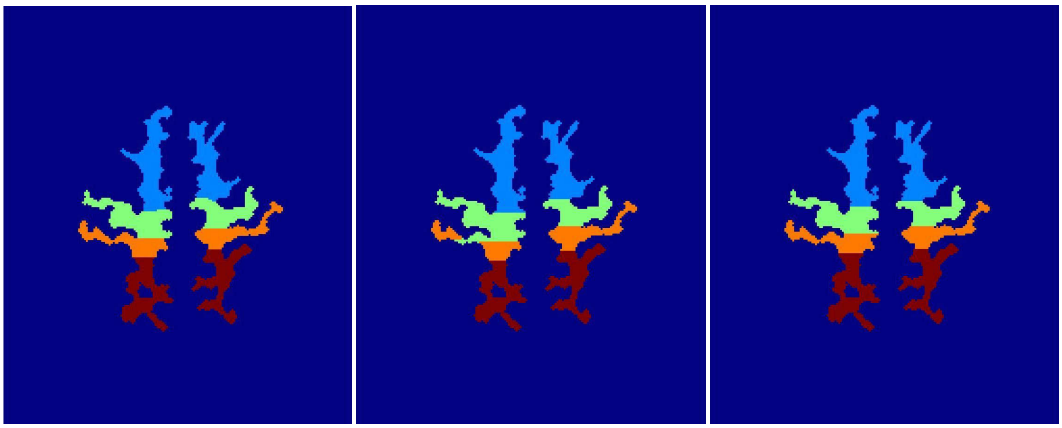

(d) ground truth (e) before refinement (f) after refinement

subject8

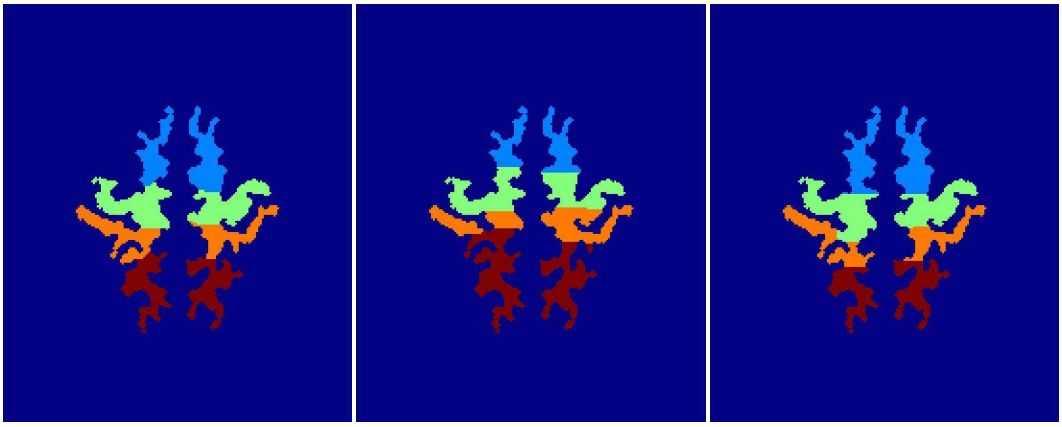

(g) ground truth (h) before refinement (i) after refinement

subject9

The effects of refine estimation for subjects 1-9 (slice 127)

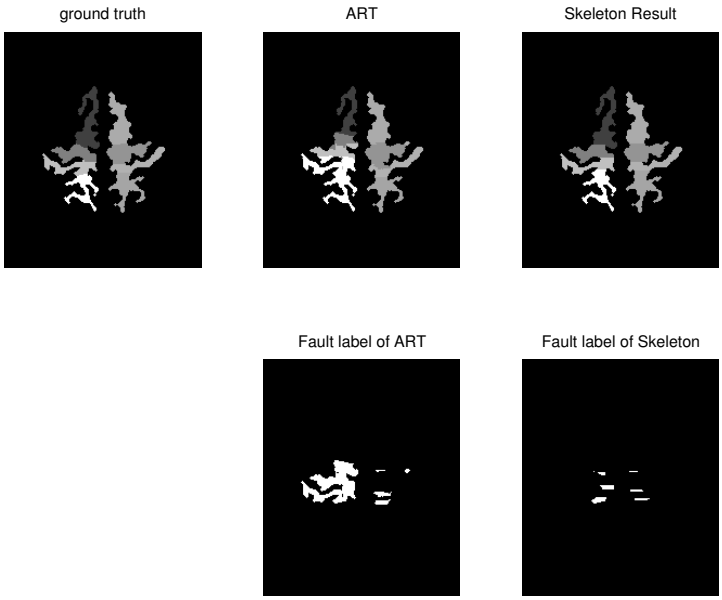

Figure 4.11: Comparing the difference between the ground truth and the proposed method and with the ART method of image 1 slice 128.

4.3.2 Time Complexity

Generally, the procedure of the skeleton algorithm includes: separating white matter from the brain, finding skeleton of subject, finding nearest skeleton to subject from the training data, transforming skeleton subject to nearest skeleton, using graph cuts for segmentation in linear time [11]. In conclusion, the time complexity of the proposed method is $O(N + |S| + K * NS)$ where N is number of pixels and $|S|$ is size of skeleton, where $|S| << N$. K is constant, and NS is number of slices of the brain.

4.4 Qualitative Evaluation

In this section, we show the final results of the proposed algorithm on two sample images of brain and compare them with the ground truth and with the ART results. Figure 4.11 and Figure 4.12 depict these results. The figures on the bottom represent the difference map between the result using skeleton method and that using the ART with the ground truth.

Figure 4.11 and Figure 4.12 show an outstanding performance in precentral

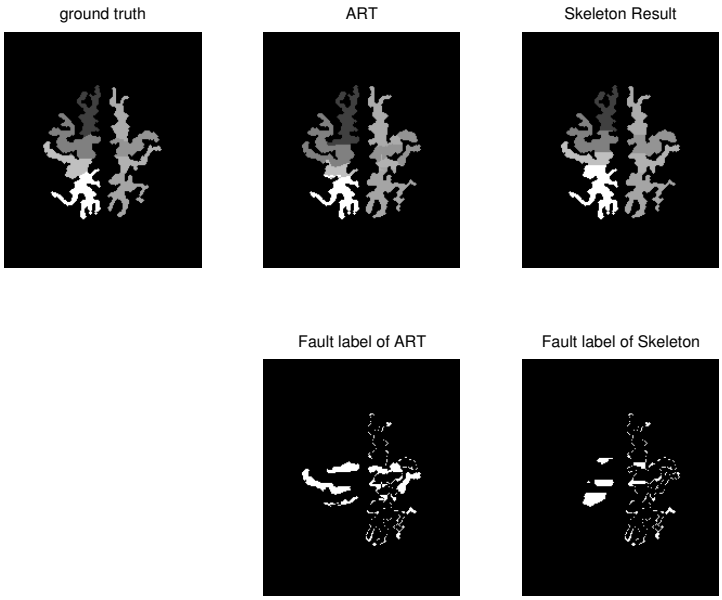

Figure 4.12: Comparing the difference between the ground truth and the proposed method and with the ART method of image 9 slice 125.

and post central segments for our proposed method against the ART. Obviously, the proposed method recognizes boundary segments better than the ART method; Area overlap and false positive results comparison between ART and the proposed method demonstrates this claim. For example, for the left side of superior, the area overlap result of the ART method is one while its false positive error is high.

Chapter 5

Conclusions and Future Work

In this thesis we addressed the problem of segmenting upper parts of the human brain into anatomical regions including the precentral, postcentral, superior frontal and superior parietal lobule. The outcome of this segmentation is essential to some disease diagnosis such as Amyotrophic Lateral Sclerosis disease in which the upper and lower motor neurons are degenerated.

The basis of our works is to use the shape of white matter in upper slices of the brain. We proposed a new method to extract a high-level information of white matter by calculating the skeleton, medial axis, in a robust and noise invariant way. Other methods to extract the skeleton of a shape are not very robust to noise which leads to poor performance if we apply them to these kinds of images. Another advantage of our proposed method is its efficiency which is linear in terms of the number of pixels in the image.

Then we search for similar images that are manually segmented by experts to find the closest brain in terms of shape and curvatures. To solve this problem we compared the extracted skeleton of the input image with all of the images in our training data set and chose the closest one. After that, we used regular methods to find the best transformation that registers our input images into the same space of the chosen image by optimizing a cost function.

The achieved results by this step was not satisfying. To refine the results to acceptable results we used graph cuts optimization and applied some constraints including continuity of regions and their sizes.

Then in chapter 4 we evaluated our proposed method by comparing our results

with ground truth which was obtained by manually segmenting the images by experts. Also, we compared our results with one of the state-of-the-art registration and segmentation methods, ART, and showed that our method outperforms the latter.

Also we analyzed the time complexity of our proposed method and showed that it is very efficient and the training dataset can easily be increased to achieve better results.

For future works, one can expand this project in several directions, and one of the most important ones is to generalize this method to extract 3D skeletons instead of 2D. By calculating the skeleton in 3D, we can solve the problem of registration for all slices at once. Also, a 3D skeleton has the advantage of being invariant to rotation. In other words, if the MR image has been rotated the 2D methods will lose accuracy.

Another possible way to improve is to use more complex methods of registration. In this work we used affine transformations to find the best registration which is very fast. But because our method generates a skeleton which is represented by a set of points, one can use more complex examples without losing time efficiency.

Increasing the number of training sets should increase accuracy as well because we used them to find the labels and having more training data should increase the chance of finding a better image for registration.

Bibliography

[1] Babak A Ardekani, Stephen Guckemus, Alvin Bachman, Matthew J Hoptman, Michelle Wojtaszek, and Jay Nierenberg. Quantitative comparison of algorithms for inter-subject registration of 3d volumetric brain mri scans. *Journal of neuroscience methods*, 142(1):67–76, 2005.

[2] John Ashburner and Karl J Friston. Unified segmentation. *Neuroimage*, 26(3):839–851, 2005.

[3] M Stella Atkins and Blair T Mackiewich. Fully automatic segmentation of the brain in mri. *Medical Imaging, IEEE Transactions on*, 17(1):98–107, 1998.

[4] Brian B Avants, Charles L Epstein, Murray Grossman, and James C Gee. Symmetric diffeomorphic image registration with cross-correlation: evaluating automated labeling of elderly and neurodegenerative brain. *Medical image analysis*, 12(1):26–41, 2008.

[5] Caroline Baillard, Pierre Hellier, and Christian Barillot. Segmentation of brain 3d mr images using level sets and dense registration. *Medical image analysis*, 5(3):185–194, 2001.

[6] Miguel Angel Gonzalez Ballester, Andrew P Zisserman, and Michael Brady. Estimation of the partial volume effect in mri. *Medical Image Analysis*, 6(4):389–405, 2002.

[7] Dr Samir Kumar Bandhyopadhyay and Tuhin Utsab Paul. Segmentation of brain mri image–a review. *International Journal of Advanced Research in Computer Science and Software Engineering*, 2(3), 2012.

[8] Amine M Bensaid, Lawrence O Hall, James C Bezdek, Laurence P Clarke, Martin L Silbiger, John Arrington, Reed F Murtagh, et al. Validity-guided (re) clustering with applications to image segmentation. *Fuzzy Systems, IEEE Transactions on*, 4(2):112–123, 1996.

[9] Mahua Bhattacharya and Arpita Das. A study on seeded region based improved watershed transformation for brain tumor segmentation. *The XXIX General Assembly of the Int Union of Radio Science*, 2008.

[10] Harry Bium. A transformation for extracting new descriptors of shape.

[11] Yuri Boykov and Vladimir Kolmogorov. An experimental comparison of min-cut/max-flow algorithms for energy minimization in vision. *Pattern Analysis and Machine Intelligence, IEEE Transactions on*, 26(9):1124–1137, 2004.

[12] David J Brenner and Eric J Hall. Computed tomographyan increasing source of radiation exposure. *New England Journal of Medicine*, 357(22):2277–2284, 2007.

[13] Korbinian Brodmann. *Brodmann's: Localisation in the Cerebral Cortex*. Springer Science & Business Media, 2007.

[14] Antoni Buades, Bartomeu Coll, and Jean-Michel Morel. A non-local algorithm for image denoising. In *Computer Vision and Pattern Recognition, 2005. CVPR 2005. IEEE Computer Society Conference on*, volume 2, pages 60–65. IEEE, 2005.

[15] HM Chan, Albert Chung, Simon CH Yu, and William M Wells III. 2d-3d vascular registration between digital subtraction angiographic (dsa) and magnetic resonance angiographic (mra) images. In *Biomedical Imaging: Nano to Macro, 2004. IEEE International Symposium on*, pages 708–711. IEEE, 2004.

[16] Herng-Hua Chang and Daniel J Valentino. An electrostatic deformable model for medical image segmentation. *Computerized Medical Imaging and Graphics*, 32(1):22–35, 2008.

[17] Ping-Lin Chang and Wei-Guang Teng. Exploiting the self-organizing map for medical image segmentation. In *Computer-Based Medical Systems, 2007. CBMS'07. Twentieth IEEE International Symposium on*, pages 281–288. IEEE, 2007.

[18] Ming-Chang Chiang, Rebecca Dutton, Kiralee M Hayashi, Arthur W Toga, Oscar L Lopez, Howard J Aizenstein, James T Becker, Paul M Thompson, et al. Fluid registration of medical images using jensen-renyi divergence reveals 3d profile of brain atrophy in hiv/aids. In *Biomedical Imaging: Nano to Macro, 2006. 3rd IEEE International Symposium on*, pages 193–196. IEEE, 2006.

[19] Matthew C Clark, Lawrence O Hall, Dmitry B Goldgof, Robert Velthuizen, F Reed Murtagh, and Martin S Silbiger. Automatic tumor segmentation using knowledge-based techniques. *Medical Imaging, IEEE Transactions on*, 17(2):187–201, 1998.

[20] LP Clarke, RP Velthuizen, MA Camacho, JJ Heine, M Vaidyanathan, LO Hall, RW Thatcher, and ML Silbiger. Mri segmentation: methods and applications. *Magnetic resonance imaging*, 13(3):343–368, 1995.

[21] D Louis Collins, Colin J Holmes, Terrence M Peters, and Alan C Evans. Automatic 3-d model-based neuroanatomical segmentation. *Human brain mapping*, 3(3):190–208, 1995.

[22] Jason J Corso, Eitan Sharon, Shishir Dube, Suzie El-Saden, Usha Sinha, and Alan Yuille. Efficient multilevel brain tumor segmentation with integrated bayesian model classification. *Medical Imaging, IEEE Transactions on*, 27(5):629–640, 2008.

[23] Anders M Dale, Bruce Fischl, and Martin I Sereno. Cortical surface-based analysis: I. segmentation and surface reconstruction. *Neuroimage*, 9(2):179–194, 1999.

[24] Carl De Boor. A practical guide to splines. *Mathematics of Computation*, 1978.

[25] Rahul S Desikan, Florent Ségonne, Bruce Fischl, Brian T Quinn, Bradford C Dickerson, Deborah Blacker, Randy L Buckner, Anders M Dale, R Paul Maguire, Bradley T Hyman, et al. An automated labeling system for subdividing the human cerebral cortex on mri scans into gyral based regions of interest. *Neuroimage*, 31(3):968–980, 2006.

[26] Christophe Destrieux, Bruce Fischl, Anders Dale, and Eric Halgren. Automatic parcellation of human cortical gyri and sulci using standard anatomical nomenclature. *Neuroimage*, 53(1):1–15, 2010.

[27] Haixia Du and Hong Qin. Medial axis extraction and shape manipulation of solid objects using parabolic pdes. In *Proceedings of the ninth ACM symposium on Solid modeling and applications*, pages 25–35. Eurographics Association, 2004.

[28] Aly A Farag, Mohamed N Ahmed, Ayman El-Baz, and Hossam Hassan. Advanced segmentation techniques. In *Handbook of biomedical image analysis*, pages 479–533. Springer, 2005.

[29] Bruce Fischl, David H Salat, Evelina Busa, Marilyn Albert, Megan Dieterich, Christian Haselgrove, Andre Van Der Kouwe, Ron Killiany, David Kennedy, Shuna Klaveness, et al. Whole brain segmentation: automated labeling of neuroanatomical structures in the human brain. *Neuron*, 33(3):341–355, 2002.

[30] Bruce Fischl, Martin I Sereno, and Anders M Dale. Cortical surface-based analysis: Ii: inflation, flattening, and a surface-based coordinate system. *Neuroimage*, 9(2):195–207, 1999.

[31] Jung Leng Foo. A survey of user interaction and automation in medical image segmentation methods. *Iowa State University, Human Computer Interaction Technical Report ISU-HCI-2006-02*, 2006.

[32] Daniel S Fritsch, Stephen M Pizer, Bryan S Morse, David H Eberly, and Alan Liu. The multiscale medial axis and its applications in image registration. *Pattern recognition letters*, 15(5):445–452, 1994.

[33] Stuart Geman and Donald Geman. Stochastic relaxation, gibbs distributions, and the bayesian restoration of images. *Pattern Analysis and Machine Intelligence, IEEE Transactions on*, (6):721–741, 1984.

[34] David T Gering, W Eric L Grimson, and Ron Kikinis. *Recognizing deviations from normalcy for brain tumor segmentation*. Springer, 2002.

[35] Nelly Gordillo, Eduard Montseny, and Pilar Sobrevilla. State of the art survey on mri brain tumor segmentation. *Magnetic Resonance Imaging*, 31(8):1426–1438, 2013.

[36] Lawrence O Hall, Amine M Bensaid, Laurence P Clarke, Robert P Velthuizen, Martin S Silbiger, and James C Bezdek. A comparison of neural network and fuzzy clustering techniques in segmenting magnetic resonance images of the brain. *Neural Networks, IEEE Transactions on*, 3(5):672–682, 1992.

[37] Alexander Hammers, Richard Allom, Matthias J Koepp, Samantha L Free, Ralph Myers, Louis Lemieux, Tejal N Mitchell, David J Brooks, and John S Duncan. Three-dimensional maximum probability atlas of the human brain, with particular reference to the temporal lobe. *Human brain mapping*, 19(4):224–247, 2003.

[38] Sean M Haney, Paul M Thompson, Timothy F Cloughesy, Jeffry R Alger, and Arthur W Toga. Tracking tumor growth rates in patients with malignant gliomas: A test of two algorithms. *American Journal of Neuroradiology*, 22(1):73–82, 2001.

[39] Robert M Haralick. Image segmentation survey. *Fundamentals in computer vision, OD Faugeras, ed., Cambridge Univ. Press, Cambridge*, pages 209–224, 1983.

[40] Rolf A Heckemann, Joseph V Hajnal, Paul Aljabar, Daniel Rueckert, and Alexander Hammers. Automatic anatomical brain mri segmentation combining label propagation and decision fusion. *NeuroImage*, 33(1):115–126, 2006.

[41] Rolf A Heckemann, Shiva Keihaninejad, Paul Aljabar, Daniel Rueckert, Joseph V Hajnal, Alexander Hammers, Alzheimer's Disease Neuroimaging Initiative, et al. Improving intersubject image registration using tissue-class information benefits robustness and accuracy of multi-atlas based anatomical segmentation. *Neuroimage*, 51(1):221–227, 2010.

[42] Pierre Hellier, Christian Barillot, Isabelle Corouge, Bernard Gibaud, Georges Le Goualher, D Louis Collins, Allan Evans, Grégoire Malandain, Nicholas Ayache, Gary E. Christensen, et al. Retrospective evaluation of intersubject brain registration. *Medical Imaging, IEEE Transactions on*, 22(9):1120–1130, 2003.

[43] Sean Ho, Lizabeth Bullitt, and Guido Gerig. Level-set evolution with region competition: automatic 3-d segmentation of brain tumors. In *Pattern Recognition, 2002. Proceedings. 16th International Conference on*, volume 1, pages 532–535. IEEE, 2002.

[44] Khan M Iftekharuddin, Jing Zheng, Mohammad A Islam, and Robert J Ogg. Fractal-based brain tumor detection in multimodal mri. *Applied Mathematics and Computation*, 207(1):23–41, 2009.

[45] Tina Kapur, W Eric L Grimson, William M Wells, and Ron Kikinis. Segmentation of brain tissue from magnetic resonance images. *Medical image analysis*, 1(2):109–127, 1996.

[46] Frederick Klauschen, Aaron Goldman, Vincent Barra, Andreas Meyer-Lindenberg, and Arvid Lundervold. Evaluation of automated brain mr image segmentation and volumetry methods. *Human brain mapping*, 30(4):1310–1327, 2009.

[47] Arno Klein, Satrajit S Ghosh, Brian Avants, BT Thomas Yeo, Bruce Fischl, Babak Ardekani, James C Gee, J John Mann, and Ramin V Parsey. Evaluation of volume-based and surface-based brain image registration methods. *Neuroimage*, 51(1):214–220, 2010.

[48] Jun Kong, Jianzhong Wang, Yinghua Lu, Jingdan Zhang, Yongli Li, and Baoxue Zhang. A novel approach for segmentation of mri brain images. In *Electrotechnical Conference, 2006. MELECON 2006. IEEE Mediterranean*, pages 525–528. IEEE, 2006.

[49] Alan P Koretsky. New developments in magnetic resonance imaging of the brain. *NeuroRx*, 1(1):155–164, 2004.

[50] Sasi Kumar et al. Skull stripping and automatic segmentation of brain mri using seed growth and threshold techniques. In *2007 International Conference on Intelligent and Advanced Systems*, pages 422–426, 2007.

[51] Phooi Yee Lau, Frank CT Voon, and Shinji Ozawa. The detection and visualization of brain tumors on t2-weighted mri images using multiparameter feature blocks. In *Engineering in Medicine and Biology Society, 2005. IEEE-EMBS 2005. 27th Annual International Conference of the*, pages 5104–5107. IEEE, 2006.

[52] Gang Li, Lei Guo, Jingxin Nie, and Tianming Liu. Automatic cortical sulcal parcellation based on surface principal direction flow field tracking. *NeuroImage*, 46(4):923–937, 2009.

[53] Ning Li, Miaomiao Liu, and Youfu Li. Image segmentation algorithm using watershed transform and level set method. In *Acoustics, Speech and Signal Processing, 2007. ICASSP 2007. IEEE International Conference on*, volume 1, pages I–613. IEEE, 2007.

[54] Stan Z Li. Markov random field models in computer vision. In *Computer VisionECCV'94*, pages 361–370. Springer, 1994.

[55] Gabriele Lohmann and D Yves von Cramon. Automatic labelling of the human cortical surface using sulcal basins. *Medical image analysis*, 4(3):179–188, 2000.

[56] Jyrki MP Lötjönen, Robin Wolz, Juha R Koikkalainen, Lennart Thurfjell, Gunhild Waldemar, Hilkka Soininen, Daniel Rueckert, Alzheimer's Disease Neuroimaging Initiative, et al. Fast and robust multi-atlas segmentation of brain magnetic resonance images. *Neuroimage*, 49(3):2352–2365, 2010.

[57] Rouzbeh Maania, Yee-Hong Yanga, and Sanjay Kalrab. Texture analysis of the brain in amyotrophic lateral sclerosis.

[58] Jan Modersitzki. *FAIR: flexible algorithms for image registration*, volume 6. SIAM, 2009.

[59] Sílvia Delgado Olabarriaga and Arnold WM Smeulders. Interaction in the segmentation of medical images: A survey. *Medical image analysis*, 5(2):127–142, 2001.

[60] Francisco PM Oliveira and João Manuel RS Tavares. Medical image registration: a review. *Computer methods in biomechanics and biomedical engineering*, 17(2):73–93, 2014.

[61] Daniel Palumbo, Brian Yee, Patrick O'Dea, Shane Leedy, Satish Viswanath, and Anant Madabhushi. Interplay between bias field correction, intensity standardization, and noise filtering for t2-weighted mri. In *Engineering in Medicine and Biology Society, EMBC, 2011 Annual International Conference of the IEEE*, pages 5080–5083. IEEE, 2011.

[62] Brian Patenaude, Stephen M Smith, David N Kennedy, and Mark Jenkinson. A bayesian model of shape and appearance for subcortical brain segmentation. *Neuroimage*, 56(3):907–922, 2011.

[63] Dzung L Pham, Chenyang Xu, and Jerry L Prince. Current methods in medical image segmentation 1. *Annual review of biomedical engineering*, 2(1):315–337, 2000.

[64] Stephen M Pizer, Christina A Burbeck, James M Coggins, Daniel S Fritsch, and Bryan S Morse. Object shape before boundary shape: Scale-space medial axes. *Journal of Mathematical Imaging and Vision*, 4(3):303–313, 1994.

[65] Josien PW Pluim, JB Antoine Maintz, Max Viergever, et al. F-information measures in medical image registration. *Medical Imaging, IEEE Transactions on*, 23(12):1508–1516, 2004.

[66] Michał Postolski, Michel Couprie, and Marcin Janaszewski. Scale filtered euclidean medial axis. In *Discrete Geometry for Computer Imagery*, pages 360–371. Springer, 2013.

[67] Marcel Prastawa, Elizabeth Bullitt, Nathan Moon, Koen Van Leemput, and Guido Gerig. Automatic brain tumor segmentation by subject specific modification of atlas priors 1. *Academic radiology*, 10(12):1341–1348, 2003.

[68] Sanaz Rahimi. *A method for detecting and locating brain tumors in MRI images*. ProQuest, 2007.

[69] R Rajeswari and P Anandhakumar. Segmentation and identification of brain tumor mri image with radix4 fft techniques. *European Journal of Scientific Research*, 52(1):100–109, 2011.

[70] Maryam E Rettmann, Xiao Han, Chenyang Xu, and Jerry L Prince. Automated sulcal segmentation using watersheds on the cortical surface. *NeuroImage*, 15(2):329–344, 2002.

[71] A Sboarina, RI Foroni, A Minicozzi, L Antiga, F Lupidi, M Longhi, M Ganau, A Nicolato, GK Ricciardi, A Fenzi, et al. Software for hepatic vessel classification: feasibility study for virtual surgery. *International journal of computer assisted radiology and surgery*, 5(1):39–48, 2010.

[72] Mark Schmidt. A method for standardizing mr intensities between slices and volumes. *University of Alberta*, 2005.

[73] N Senthilkumaran and R Rajesh. Edge detection techniques for image segmentation–a survey of soft computing approaches. *International journal of recent trends in engineering*, 1(2), 2009.

[74] Stephen M Smith, Mark Jenkinson, Mark W Woolrich, Christian F Beckmann, Timothy EJ Behrens, Heidi Johansen-Berg, Peter R Bannister, Marilena De Luca, Ivana Drobnjak, David E Flitney, et al. Advances in functional and structural mr image analysis and implementation as fsl. *Neuroimage*, 23:S208–S219, 2004.

[75] John W Snell, Michael B Merickel, James M Ortega, John C Goble, James R Brookeman, and Neal F Kassell. Segmentation of the brain from 3d mri using a hierarchical active surface template. In *Medical Imaging 1994*, pages 2–9. International Society for Optics and Photonics, 1994.

[76] Wlad T Sobol. Recent advances in mri technology: Implications for image quality and patient safety. *Saudi Journal of Ophthalmology*, 26(4):393–399, 2012.

[77] M Spitzner and Ruben Gonzalez. Shape peeling for improved image skeleton stability. In *Acoustics, Speech and Signal Processing (ICASSP), 2015 IEEE International Conference on*, pages 1508–1512. IEEE, 2015.

[78] Sookpotharom Supot, Chaichana Thanapong, Pintavirooj Chuchart, and Sangworasil Manas. Segmentation of magnetic resonance images using discrete curve evolution and fuzzy clustering. In *Integration Technology, 2007. ICIT'07. IEEE International Conference on*, pages 697–700. IEEE, 2007.

[79] Ralf Tetzlaff, Tobias Schwarz, Hans-Ulrich Kauczor, Hans-Peter Meinzer, Michael Puderbach, and Monika Eichinger. Lung function measurement of single lungs by lung area segmentation on 2d dynamic mri. *Academic radiology*, 17(4):496–503, 2010.

[80] Dan Tian and Linan Fan. A brain mr images segmentation method based on som neural network. In *Bioinformatics and Biomedical Engineering, 2007. ICBBE 2007. The 1st International Conference on*, pages 686–689. IEEE, 2007.

[81] Thanh N Tran, Ron Wehrens, and Lutgarde MC Buydens. Clustering multispectral images: a tutorial. *Chemometrics and Intelligent Laboratory Systems*, 77(1):3–17, 2005.

[82] Nathalie Tzourio-Mazoyer, Brigitte Landeau, Dimitri Papathanassiou, Fabrice Crivello, Olivier Etard, Nicolas Delcroix, Bernard Mazoyer, and Marc Joliot. Automated anatomical labeling of activations in spm using a macroscopic anatomical parcellation of the mni mri single-subject brain. *Neuroimage*, 15(1):273–289, 2002.

[83] Balakrishnan Varadarajan, Carol Reiley, Henry Lin, Sanjeev Khudanpur, and Gregory Hager. Data-derived models for segmentation with application to surgical assessment and training. In *Medical Image Computing and Computer-Assisted Intervention–MICCAI 2009*, pages 426–434. Springer, 2009.

[84] Esther Verstraete, Martijn P Van Den Heuvel, Jan H Veldink, Niels Blanken, René C Mandl, Hilleke E Hulshoff Pol, and Leonard H van den Berg. Motor network degeneration in amyotrophic lateral sclerosis: a structural and functional connectivity study. 2010.

[85] Sara Fernández Vidal, Eric Bardinet, Grégoire Malandain, Sergio Damas, and Nicolas Pèrez De La Blanca Capilla. Object representation and comparison inferred from its medial axis. In *Pattern Recognition, 2000. Proceedings. 15th International Conference on*, volume 1, pages 712–715. IEEE, 2000.

[86] C Vijayakumar and Damayanti Chandrashekhar Gharpure. Development of image-processing software for automatic segmentation of brain tumors in mr images. *Journal of medical physics/Association of Medical Physicists of India*, 36(3):147, 2011.

[87] Williams M Wells III, W Eric L Grimson, Ron Kikinis, and Ferenc A Jolesz. Adaptive segmentation of mri data. *Medical Imaging, IEEE Transactions on*, 15(4):429–442, 1996.

[88] Jay West, J Michael Fitzpatrick, Matthew Y Wang, Benoit M Dawant, Calvin R Maurer Jr, Robert M Kessler, Robert J Maciunas, Christian Barillot, Didier Lemoine, Andre Collignon, et al. Comparison and evaluation of

retrospective intermodality brain image registration techniques. *Journal of computer assisted tomography*, 21(4):554–568, 1997.

[89] Koon-Pong Wong. Medical image segmentation: methods and applications in functional imaging. In *Handbook of Biomedical Image Analysis*, pages 111–182. Springer, 2005.

[90] Roger P Woods, Scott T Grafton, Colin J Holmes, Simon R Cherry, and John C Mazziotta. Automated image registration: I. general methods and intrasubject, intramodality validation. *Journal of computer assisted tomography*, 22(1):139–152, 1998.

[91] Roger P Woods, Scott T Grafton, John DG Watson, Nancy L Sicotte, and John C Mazziotta. Automated image registration: Ii. intersubject validation of linear and nonlinear models. *Journal of computer assisted tomography*, 22(1):153–165, 1998.

[92] Kai Xie, Jie Yang, ZG Zhang, and YM Zhu. Semi-automated brain tumor and edema segmentation using mri. *European Journal of Radiology*, 56(1):12–19, 2005.

[93] Zhennan Yan, Shaoting Zhang, Xiaofeng Liu, Dimitris N Metaxas, and Albert Montillo. Accurate segmentation of brain images into 34 structures combining a non-stationary adaptive statistical atlas and a multi-atlas with applications to alzheimer's disease. In *Biomedical Imaging (ISBI), 2013 IEEE 10th International Symposium on*, pages 1202–1205. IEEE, 2013.

[94] Jianhua Yao. Image processing in tumor imaging. *New techniques in oncologic imaging*, pages 79–102, 2006.

[95] Michael A Yassa and Craig EL Stark. A quantitative evaluation of cross-participant registration techniques for mri studies of the medial temporal lobe. *Neuroimage*, 44(2):319–327, 2009.

[96] Terry S Yoo, Michael J Ackerman, William E Lorensen, Will Schroeder, Vikram Chalana, Stephen Aylward, Dimitris Metaxas, and Ross Whitaker. Engineering and algorithm design for an image processing api: a technical report on itk-the insight toolkit. *Studies in health technology and informatics*, pages 586–592, 2002.

[97] Sung Won Yoon, Hai Kwang Lee, Jeong Hoon Kim, and Myoung Ho Lee. Medical endoscopic image segmentation using snakes. *IEICE TRANSACTIONS on Information and Systems*, 87(3):785–789, 2004.

[98] S Yoshida, DW Mulder, LT Kurland, C Chu, and H Okazaki. Follow-up study on amyotrophic lateral sclerosis in rochester, minn., 1925 through 1984. *Neuroepidemiology*, 5(2):61–70, 1986.